Role of the neutral amino acid transporter SLC7A10 in adipocyte lipid storage, obesity and insulin resistance

Regine Å. Jersin[1,2], Divya Sri Priyanka Tallapragada[1,2], André Madsen[1,2], Linn Skartveit[1,2], Even Fjære[3], Adrian McCann[4], Laurence Dyer[1,2], Aron Willems[1,2], Jan-Inge Bjune[1,2], Mona S. Bjune[1,2], Villy Våge[2,5], Hans Jørgen Nielsen[6], Håvard Luong Thorsen[7], Bjørn Gunnar Nedrebø[1,8], Christian Busch[9], Vidar M. Steen[10,11], Matthias Blüher[12], Peter Jacobson[13], Per-Arne Svensson[13], Johan Fernø[1,2], Mikael Rydén[14], Peter Arner[14], Ottar Nygård[1,15], Melina Claussnitzer[1,16,17], Ståle Ellingsen[3,18], Lise Madsen[3,19], Jørn V. Sagen[1,2,20], Gunnar Mellgren[1,2], Simon N. Dankel[1,2*]

[1] Mohn Nutrition Research Laboratory, Department of Clinical Science, University of Bergen, N-5020 Bergen, Norway.

[2] Hormone Laboratory, Haukeland University Hospital, N-5021 Bergen, Norway.

[3] Institute of Marine Research, Postboks 1870, Nordnes, N-5817, Bergen, Norway

[4] Bevital A/S, Laboratoriebygget, 5021 Bergen, Norway

[5] Center of Health Research, Førde Hospital Trust, N-6812 Førde, Norway.

[6] Department of Surgery, Voss Hospital, Bergen Health Trust, N-5704 Voss, Norway.

[7] Department of Surgery, Haugesund Hospital, N-5528 Haugesund, Norway.

[8] Department of Medicine, Haugesund Hospital, N-5528 Haugesund, Norway.

[9] Plastikkirurg1 AS, Sandslimarka 61-63, N-5254 Bergen, Norway.

[10] NORMENT, K.J. Jebsen Center for Psychosis Research, Department of Clinical Science, University of Bergen, N-5020 Bergen, Norway.

[11] Dr. E. Martens Research Group for Biological Psychiatry, Department of Medical genetics, Haukeland University Hospital, N-5021 Bergen, Norway.

[12] Clinic for Endocrinology and Nephrology, Medical Research Center, D-04103 Leipzig, Germany.

[13] Institute of Medicine, The Sahlgrenska Academy at the University of Gothenburg, SE-405 30 Gothenburg, Sweden.

[14] Department of Medicine (H7), C2-94, Karolinska Institutet at Karolinska University Hospital, Huddinge, 141 86, Stockholm, Sweden.

[15] Department of Heart Disease, Haukeland University Hospital, N-5021 Bergen, Norway.

[16] Broad Institute of MIT and Harvard, Cambridge, Massachusetts, USA.

[17] Department of Medicine, Beth Israel Deaconess Medical Center, Harvard Medical School, Boston MA, USA

[18] Department of Biological Sciences, University of Bergen, NO-5020 Bergen, Norway.

[19] Department of Biology, University of Copenhagen, Universitetsparken 13, 2100 Copenhagen, Denmark.

[20] Bergen Stem Cell Consortium, Haukeland University Hospital, N-5021 Bergen, Norway.

Abbreviated title: Adipocyte SLC7A10, lipid storage and insulin resistance

Tweet: Jersin et al. report on SLC7A10, a new #adipocyte factor that modulates #lipid storage and #insulin resistance. Implicates importance of adipose serine transport for protection against #oxidative stress, #fat storage and risk of #type 2 diabetes @UiB @medofak_uib @simondankel

Word count: 5193

* Corresponding author: Simon N. Dankel, PhD
Department of Clinical Science
University of Bergen
Haukeland University Hospital
N-5021 Bergen, Norway
Phone: (+47 94 30 86 37)
e-mail: simon.dankel@uib.no

ABSTRACT

Elucidation of mechanisms that govern lipid storage, oxidative stress and insulin resistance may lead to improved therapeutic options for type 2 diabetes and other obesity-related diseases. Here, we find that adipose expression of the small neutral amino acid transporter SLC7A10, also known as alanine-serine-cysteine transporter 1 (ASC-1), shows strong inverse correlates with visceral adiposity, insulin resistance and adipocyte hypertrophy across multiple cohorts. Concordantly, loss of Slc7a10 function in zebrafish *in vivo* accelerates diet-induced body weight gain and adipocyte enlargement. Mechanistically, SLC7A10 inhibition in human and murine adipocytes decreases adipocyte serine uptake and total glutathione levels and promotes reactive oxygen species (ROS) generation. Conversely, SLC7A10 overexpression decreases ROS generation and increases mitochondrial respiratory capacity. RNA-sequencing revealed consistent changes in gene expression between human adipocytes and zebrafish visceral adipose tissue following loss of SLC7A10, e.g., upregulation of *SCD* (lipid storage) and downregulation of *CPT1A* (lipid oxidation). Interestingly, ROS scavenger reduced lipid accumulation and attenuated the lipid-storing effect of SLC7A10 inhibition. These data uncover adipocyte SLC7A10 as a novel important regulator of adipocyte resilience to nutrient and oxidative stress, in part by enhancing glutathione levels and mitochondrial respiration, conducive to decreased ROS generation, lipid accumulation, adipocyte hypertrophy, insulin resistance and type 2 diabetes.

Keywords: Obesity, Insulin resistance, Adipose tissue, Amino acids, Reactive oxygen species, Lipid metabolism

INTRODUCTION

Adipocyte hypertrophy in both subcutaneous (SC) and visceral white adipose tissue (WAT) is strongly associated with whole-body insulin resistance, with or without obesity and adipose tissue (AT) inflammation (1,2), and with fatty liver, dyslipidemia, impaired mitochondrial function, and reduced insulin-stimulated glucose uptake in adipocytes (3). Experimental impairment of mitochondrial respiration and increased reactive oxygen species (ROS) generation in adipocytes reduces adipocyte insulin sensitivity (4), and the extent of mitochondrial dysfunction determines the severity of insulin resistance and type 2 diabetes (5). However, the molecular mechanisms that promote adipocyte hypertrophy and insulin resistance remain incompletely understood, and we urgently need new potential treatment targets.

SLC7A10, also known as alanine-serine-cysteine transporter 1 (ASC-1), has sodium-independent activity and high affinity for the small neutral amino acids (AAs) glycine, L-alanine, L-threonine, L-cysteine, L-serine and D-serine (6,7). *SLC7A10* is highly expressed in certain regions of the brain, and is being explored as a therapeutic target in neuropsychiatric disorders (e.g., schizophrenia) (8).

A previous report showed selective expression of *SLC7A10* in white but not beige or brown adipocytes, with 5-fold higher expression in AT compared to the highest expressing parts of the brain, and diminished expression in other tissues (9). However, the possible role of SLC7A10 in metabolic regulation has not been explored.

While AAs known to be transported by SLC7A10 in the brain, e.g., serine, glycine and cysteine, have central roles in one-carbon metabolism, the methionine cycle, glutathione synthesis and redox balance (6,7,10,11), the AAs carried by SLC7A10 in adipocytes and the consequent metabolic effects are unknown. By transcriptome screens and interrogation of several human obesity cohorts along with functional experiments, we here uncover SLC7A10 as an important novel regulator of core metabolic functions in white adipocytes, providing new insight into the development of obesity and insulin resistance.

RESEARCH DESIGN AND METHODS

Human cohorts and samples

Anthropometric data are summarized in Table 1 (7 cohorts).

RNA and gene expression analyses

Whole AT was homogenized or fractionated into isolated adipocytes or stromal vascular fraction (SVF), and RNA was purified, as described previously (12). Global gene expression in whole AT was measured by microarrays as described previously for the BPD-Fat cohort (13), Sib Pair cohort (14), VLCD study (baseline data) (15) and RIKEN cohort (16). qPCR was performed with SYBR Green dye following cDNA synthesis using high-capacity cDNA reverse transcription kit (Applied Biosystems) (**Supplementary Table 1**).

Human cell cultures

Primary human adipocyte cultures

Human liposuction aspirates from the abdomen and flanks were collected with informed consent from donors undergoing cosmetic surgery at Aleris medical center and Plastikkirurg1 in Bergen, Norway. The donors comprised 18 women and 1 man between 21 and 68 years of age (46.3±12.4) and with BMI between 24.3 and 32.8 (27.9±2.7), all free of diabetes and otherwise healthy (**Supplementary Table 2**).

Isolation and culturing of human stromal vascular fraction

The stromal vascular fraction (SVF) from SC AT was isolated as previously described (17) with some modifications. Briefly, KRP-buffer containing Liberase Blendzyme 3 (Roche) and DNase was added to the liposuction aspirate. Following a 1-hour incubation at 37°C, the digested fat tissue was filtered,washed with 0.9% NaCl and centrifugated.. Red blood cells were lysed (NH_4Cl (155 mM), K_2HPO_4 (5.7 mM) and EDTA (0.1 mM)). Preadipocytes were seeded and cultured in GlutaMAX DMEM (Thermo Fisher) supplemented with 10% fetal bovine serum (FBS) and 50 µg/ml gentamicin (Sigma) and grown at 37°C with 5% CO_2. The following day, differentiation of primary human adipose cells (human adipose stromal cells, hASCs) was induced by supplementing the culture medium with 33 µM biotin, 1 nM triiodothyronine, 17 µM DL-pantothenate, 10 µg/ml

transferrin, 66 nM insulin, 100 nM cortisol, 15 mM Hepes and 10 μM rosiglitazone. Rosiglitazone was discontinued after 6 days and terminal differentiation was defined at 12-13 days.

Mouse cell cultures and primary cells

3T3-L1 mouse preadipocytes were cultured and differentiated as described previously (18).

SLC7A10 inhibitors

BMS-466442 (AOBIOUS), referred to as SLC7A10 inhibitor 1 (19), and Lu AE00527, referred to as SLC7A10 inhibitor 2 (20), were used to inhibit SLC7A10 function in *in vitro* cell culture experiments at a standard final concentration of 10 μM. The latter inhibitor was provided by H. Lundbeck A/S (Valby, Denmark).

Gene expression analysis

Total RNA from human and mouse cell cultures was isolated using RNeasy kit (QIAGEN) and quality checked by QIAxpert spectrophotometer (QIAGEN) prior to cDNA synthesis with 200 ng RNA input using a high-capacity cDNA reverse transcription kit (Applied Biosystems). cDNA was analyzed by Lightcycler480 (Roche) quantitative real-time PCR using SYBR Green dye (Roche) and target primers (**Supplementary Table 1**). Relative mRNA expression was determined by standard curves and normalized to reference gene (*HPRT* or *Rps13*). Prior to RNA sequencing, samples were DNase treated and RNA integrity number (RIN>9) was confirmed by Bioanalyzer (Agilent). cDNA libraries were generated using TruSeq Stranded mRNA Library Prep kit and sequenced by Illumina Hiseq 4000. Reads were mapped against the Human genome (GrCH38) using HiSat (Version 2.1.0), tabulated by featureCounts (Version 1.5.2) and analyzed using DESeq2 (Version 1.22.2).

Co-expression, gene ontology (GO) and pathway analysis

Co-expression analysis was performed based on global gene expression data for human adipocytes isolated directly from biopsies of 12 lean and 12 obese patients (ADIPO cohort). Pearson correlation coefficients were calculated for correlations between *SLC7A10* mRNA and all other transcripts globally (around 47,000 probes, including 21,000 individual genes) across the 24 patients. Genes with correlation coefficients (β) $\beta>0.65$ or $\beta<-0.65$ were analyzed using

PANTHER Gene List Analysis tool (http://www.pantherdb.org/) to perform statistical overrepresentation test (binomial statistics, Bonferroni-corrected for multiple testing). RNA-seq results from hASCs were analyzed by PANTHER (v.14.0), utilizing Fisher's exact test (21).

Transfection:

Transfection with mouse Slc7a10 expression plasmid was performed using the transfection reagent TransIT-L1, following the manufacturer's protocol (Mirus Bio LCC). 2.0 µg of Slc7a10 plasmid or empty vector was used per ml medium (**Supplementary Table 3**).

Western blotting

Cells were lysed in RIPA buffer (Thermo Fisher) containing EDTA-free protease inhibitor cocktail (Roche) and PhosphoStop (Sigma). Protein content in the lysates was determined using DC protein assay (Bio-Rad), loaded onto 4-20% TGX gels (Bio-Rad) and subjected to SDS-PAGE prior to transfer to nitrocellulose membrane. Membranes were developed using Femto solution (Thermo Scientific) and target protein amount relative to endogenous control was quantified by densitometry.

Amino acid quantification

Extracellular (medium) AA concentrations were assayed by GC-MS/MS (Agilent) (22). Flux was calculated based on AA concentration in unconditioned and conditioned medium.

Radiolabeled amino acid uptake assays

AA uptake was measured in sodium-free assay buffer, as described previously (19), using unlabeled controls (D- or L-Serine, final concentration 10 mM) and stock solutions of D-[^{3}H] Serine (15 Ci/mmol) and L-[^{14}C] Serine (100mCi/mmol) (Perkin Elmer). Sample radioactivity was measured as 5-minute averaged CPM (QuantaSmart software).

Mitochondrial respiration assay

Cellular respiration was measured by the Seahorse Mito Stress Test kit and XF96 analyzer (Agilent). Preadipocytes were seeded in gelatin-coated (0.1% w/v) microplates and differentiated. Cells were washed and treated in XF base medium supplemented with L-glutamine (2 mM),

sodium pyruvate (2 mM) and glucose (10 mM) and incubated in a CO_2-free incubator for 1 hour. Oxygen consumption rate (OCR) data were normalized to numbers of cells per well, measured by Hoechst staining.

Lipid staining

Lipid accumulation was assessed by Oil red O (ORO) staining as described previously (23).

Radiolabeled glucose uptake assays

Adipocytes were washed with PBS and incubated overnight in glucose reduced DMEM w/wo treatment. Subsequently, cells were starved in glucose-free medium w/wo treatment for 2.5 hours. Insulin (final concentration 10nM) was added to indicated wells for 30 minutes prior to the assay. Deoxy-D-[^{14}C]-Glucose (57.7mCi/mmol) (Perkin Elmer) was added for 30 minutes and incubated at 37 ºC. Cells were placed on ice,washed and lysates were collected in Ultima Gold fluid cartridges (Perkin Elmer). Isotope retention in lysate was measured as 5-minute averaged counts per minute (CPM) (QuantaSmart software) in a scintillation counter.

Reactive Oxygen Species (ROS) assay

Adipocytes were incubated for 30 minutes with or without 5µM CM-H2DCFDA as described previously (24). Cells were washed and incubated in Krebs-ringer bicarbonate (KRB) buffer or sodium-free assay buffer, with indicated compounds, followed by measurement of fluorescent emission of oxidized H2DCFDA probe (538nm following 485nm excitation) using a SpectraMax Gemini EM (Molecular Devices) plate reader at 37 °C.

Glutathione assay

Total glutathione was measured using the GSH/GSSG-Glo^{TM} Assay (Promega), according to the manufacturer's protocol. Briefly, cells were lysed with glutathione lysis reagent and incubated in luciferin generation reagent for 30 minutes at RT. Samples were incubated for 15 minutes following addition of luciferin detection reagent. Luminescence was measured using FLUOstar OPTIMA EM (Thermo Fisher Scientific).

In vivo Zebrafish model

Heterozygous slc7a10b loss-of-function *Danio rerio* (zebrafish) were obtained from The Zebrafish Model Organism Database (ZFIN, genomic feature sa15382) and crossed to obtain homozygote and wild-type (WT) zebrafish.

Genotyping

Genomic DNA was extracted from caudal fin biopsies of mature Zebrafish using DNeasy kit (QIAGEN). For genotyping, a 298 bp region of the *slc7a10b* gene containing the intron splice site A→T mutation was amplified by PCR using Platinum Taq High Fidelity DNA Polymerase (Invitrogen) and the flanking primers 5'-TCGCCTACTTCTCCTCCATG-3' (forward) and 5'-TTCCCAAGTCCTCCTGATGC-3' (reverse). Samples were subjected to endonuclease digestion using the restriction enzyme Acc*I* (New England Biolabs) prior to band separation by agarose gel electrophoresis. Genotypes were determined based on signature fragment digestion of the PCR product where the A→T mutation abolished the Acc*I* recognition cleavage site.

Selection and genomic features

The ZFIN genomic feature sa15382 zebrafish used in this study exhibited a p
oint mutation in the conserved 3' splice site between exon 6 and 7 in the *slc7a10b* gene (ENSDART00000073398.5). This A→T mutation disrupts the dinucleotide splice site, and the intron between exon 6 and 7 is not spliced during maturation of the mRNA. Thus, the mRNA length is increased and the slc7a10b protein product is inactive. Heterozygous larvae were raised and bred to obtain zebrafish homozygous for this mutation. Due to the large variation in body weight between male and female zebrafish in a pilot study, the overfeeding study was performed using male zebrafish.

Husbandry

4-month-old male zebrafish were housed in 3-liter tanks (on average 20 per tank) with a recirculating system (Aquatic Habitats, Pentair AES) at 28.5±1 °C and pH 7.5±0.3, with 10% daily water exchange, electrical conductivity of 500 ±50µs, and a 14h light and 10h dark circadian cycle. Zebrafish were fed 8.2 mg Gemma Micro 500 (Skretting, USA) per day, divided over three timepoints (at 8am, noon and 4pm), in addition to freshly hatched *Artemia* (3 drops of a 24h *Artemia* culture) once per day. Gemma Micro 500, which the zebrafish were fed both under normal

and overfeeding conditions, consisted of fishmeal, lecithin, wheat gluten, zebrafish oil, vitamins and mineral premixes and betaine, containing 59% (w/w) protein sources and 14% (w/w) lipids (containing 14% omega-3 fatty acids).

Overfeeding

Three adult zebrafish were held per 1.5-liter tank, in total 33 WT and 39 loss-of-function zebrafish. To promote weight gain, 12.3 mg feed per zebrafish per day (50% more feed than normal) was given for the first 3 weeks and 16.4 mg (100% more feed than normal) for the last 5 weeks of the overfeeding study. The circulation system was turned off for 5 minutes before and 30 minutes after each feeding, allowing consumption of all supplied food. Zebrafish were otherwise fed as under normal conditions (described above).

Measuring and weighing

Zebrafish length and weight was recorded at the start and the end of the study, while weight was also measured after 3 and 6 weeks. Since it was not feasible to control the feed intake of each individual fish, recorded data, and tissue samples from the three zebrafish in each tank were combined to obtain an average for each tank. Before all handelling, each zebrafish was sedated using 75 mg/L to 200 mg/L Tricain mesylate (Pharmaq).

Sample collection and RNA sequencing

Following sacrifice, tissue biopsies from three zebrafish in each tank were pooled together and snap-frozen in liquid nitrogen. Adipose and liver biopsies were fixed in 4% (v/v) paraformaldehyde in 0.1 M phosphate buffer for 12 hours and paraffin embedded after gradual dehydration as described previously (25). Slice sections of 5µm were stained with hematoxylin and eosin, and adipocyte size was analyzed and quantified using Image J open-source software as described elsewhere (18). Total RNA from zebrafish visceral adipose tissue (VAT) was prepared for RNA-seq as described for human adipose cultures, as well the generation of cDNA libraries. Sample reads were mapped against the Zebrafish genome (GRCz10) using HiSat (Version 2.05), tabulated by featureCounts (Version 1.5.2) and analyzed using DESeq2 (version 1.22.1).

Statistics

Differences between groups in human cohort data were analyzed using paired t-test, one or two-way ANOVA, and are presented as mean ± SD. For Pearson correlation and multiple regression analyses, adjustments for BMI and sex are indicated. Differences between groups in cell culture experiments were assessed using two-tailed unpaired student's t-test or one-way ANOVA with Dunnett's or Sidak's correction for multiple comparisons. Sample data from empirical experiments were assumed to be normally distributed and results are presented as mean ± SD, except for the Seahorse data which are presented as geometric mean ± 95% confidence interval. All data were subjected to a Box Whiskers Tukey test to detect and remove outliers. Statistical significance was calculated in GraphPad or with the R bio conductor package limma v3.34.9. Statistical details and the number of biological samples (n) for all experiments are provided in the figure legends. For cell experiments, n annotates the number of parallel wells per treatment. For zebrafish samples, n annotates the number of zebrafish per treatment. For qPCR data, n annotates either the number of patients, or the number of wells in a cell experiment.

Study approval

All human samples analyzed in the present study were obtained with written informed consent and approval given by the respective regional ethics committees (2010/502 and 2010/3405, REC West Norway; Dnr 721-96 and S 172-02, REC in Gothenburg, Sweden; 2009/1881-31/1, 2011/1002-31/1 and 2015/530-32, Committee of Ethics at Karolinska Institutet, Stockholm, Sweden; and the Ethics Committee of the University of Leipzig, Germany).

Zebrafish were raised and cared for according to the Norwegian Animal Welfare Act guidelines, and all experiments after 5 days post fertilization (dpf) were approved by the Norwegian Food Safety Authority (FOTS ID 9199).

Data and resource availability

Datasets generated and/or analyzed during the current study are available from the corresponding author upon reasonable request. In addition, the RNA sequencing datasets in this publication have been deposited in the NCBI's Gene Expression Omnibus (26) and are accessible through GEO Series accession number GSE135156.

RESULTS

Implication of adipocyte *SLC7A10* in abdominal adiposity and insulin resistance

In transcriptome screens of adipose samples from people at the peak of extreme obesity (BPD-Fat cohort, **Table 1**), we prioritized candidate genes with concomitant differential expression in two separate disease-relevant comparisons of adipose function: visceral (omental, OM) and abdominal SC AT in extreme obesity, and before and after profound fat loss (SC AT from the same patients). This combined transcriptome screen identified 65 genes with both depot- and fat loss-dependent expression (fold change ≥ 1.5 and q-value < 0.01 cutoffs in both analyses) (**Supplementary Table 4**). Further supporting a role for many of these genes in insulin resistance, we found strong significant correlations for 27 of the 65 genes (42%) with waist-to-hip ratio (WHR) adjusted for BMI and sex, in a second cohort of 88 people (Sib Pair cohort) (**Supplementary Table 4**) (14). Among these genes, only 5 (8%) showed inverse correlations with WHR, 4 of which displayed highest expression in OM AT and up-regulation in SC AT after profound fat loss (*CIDEA*, *SLC7A10*, *GPD1L* and *HOXA5*) (**Supplementary Table 4**). Among the 27 candidates, we additionally prioritized genes with high expression in adipocytes specifically, based on a cohort containing isolated adipocytes and stromal vascular fraction (SVF) (ADIPO cohort). Calculation of adipocyte/SVF expression ratios revealed *CIDEA* and *SLC7A10* as stand-out candidates with similar expression profiles (**Figure 1A**). While previous studies have investigated functional roles of CIDEA in adipocytes (27), there is a paucity of functional data on adipocyte SLC7A10.

qPCR analysis of a larger cohort of people with severe obesity (WNOB cohort) confirmed the adipose depot- and fat-loss dependent expression pattern of *SLC7A10* (**Figure 1B**). *SLC7A10* mRNA was also higher in OM compared to SC samples in both isolated adipocytes and SVF (ADIPO cohort), but with diminished expression in SVF (**Figure 1C**). Consistent with increased SC *SLC7A10* expression after surgery-induced fat loss (**Figure 1C**), SC adipocytes and SVF from lean people showed higher expression than samples from those with obesity (**Figure 1C**). Furthermore, insulin resistant obese (IRO) patients showed lower *SLC7A10* mRNA compared to BMI-matched insulin sensitive obese (ISO) patients (28), in SC as well as OM fat (ISO cohort) (**Figure 1D**). Consistently, SC whole tissue *SLC7A10* mRNA levels showed strong inverse correlations with HOMA-IR, triacylglycerol (TAG) levels, SC adipocyte volume, WHR and visceral fat volume (**Figure 1E, Supplementary Figure 1**). On the other hand, SC *SLC7A10*

mRNA showed positive correlations with SC adipocyte number and SC abdominal fat mass when adjusting for BMI and sex (**Figure 1E, Supplementary Figure 1**). Finally, comparing patients with and without type 2 diabetes in the WNOB morbid obesity cohort, we observed decreased *SLC7A10* mRNA expression in omental as well as SC post-surgery AT (**Figure 1F**).

Loss of Slc7a10b function in zebrafish causes body weight gain and visceral adipocyte hypertrophy

To determine a potential causal role for SLC7A10 in the regulation of fat storage and adipose metabolism, we obtained zebrafish containing a splice site (loss-of-function) mutation in intron 6 of S*lc7a10* isoform b. After 2 months of overfeeding, the knockout zebrafish had on average gained 38% more body weight than their wildtype (WT) counterparts (**Figure 2A**). Assessing AT morphology, we observed on average 49% larger adipocytes in the loss-of-function zebrafish compared to WT (**Figure 2B,C**). Histological analyses of liver, which may reveal altered morphology related to impaired fatty acid oxidation (i.e., fatty liver), showed no apparent differences in cell size and lipid droplet formation between the Slc7a10b loss-of-function and WT zebrafish (**Figure 2C**).

***SLC7A10* is upregulated in mature adipocytes and regulates lipid metabolism**

We consequently explored mechanisms of the fat accretion by studying direct effects of altered SLC7A10 function in adipocytes. In differentiated mouse 3T3-L1 adipocytes and primary human adipose stromal cells (hASCs), SLC7A10 showed a marked increased mRNA and protein expression (**Figure 3A-D**. To study the consequence of decreased SLC7A10 function in adipocytes, we inhibited SLC7A10 using the selective inhibitors BMS-466442 (SLC7A10 inhibitor 1) (19,29) or Lu-AE00527 (SLC7A10 inhibitor 2) (20) during differentiation and observed increased lipid accumulation in 3T3-L1s (**Figure 3E**) as well as hASCs (**Figure 3F**) compared to controls.

Adipose SLC7A10 impairment affects energy metabolic pathways

To systematically explore SLC7A10-dependent metabolic processes, we first correlated mRNA levels of *SLC7A10* and other genes in a global transcriptome analysis of adipocytes isolated directly from human SC fat biopsies (ADIPO cohort). Subjecting the most *SLC7A10*-correlated

transcripts to gene ontology analysis, we found that genes anti-expressed to *SLC7A10* (113 unique genes, **Supplementary Table 5**) mapped primarily to cellular/developmental processes and protein transport (**Figure 4A**), and co-expressed genes (323 unique genes, **Supplementary Table 5**) to lipid metabolic processes and oxidative phosphorylation (**Figure 4A**). Moreover, RNA-seq in SLC7A10 inhibitor-treated primary human adipocytes revealed a profound transcriptome effect (**Supplementary Figure 2A-C**). Among 862 significantly downregulated genes , gene ontology analysis revealed an enrichment of genes involved in biological processes such as immune response, inflammation, extracellular matrix organization and cell differentiation (**Supplementary Figure 2D)**. Among 1,113 significantly upregulated genes there were striking enrichments for isopentenyl diphosphate biosynthetic process (26-fold), NADPH regeneration (26-fold), pentose phosphate shunt (26-fold), triglyceride biosynthetic process (9.3-fold) and glutathione metabolic processes (8.2-fold) (**Supplementary Figure 2D**), indicating mechanisms that fueled lipid storage. Additionally, by pathway analysis we found a marked enrichment of genes involved in ATP synthesis (16-fold), TCA cycle (13-fold) and cholesterol biosynthesis (12-fold) among upregulated genes, and in, e.g., glycolysis and angiogenesis for the downregulated genes (**Figure 4B,C**).

Global gene expression in VAT from Slc7a10b loss-of-function and WT zebrafish was also assayed by RNA-seq. Visualization of RNA-seq reads identified the expected mutation in the splice site of exon 6 (**Supplementary Figure 3A**). Of note, mutants exhibited increased mRNA levels of the defective *Slc7a10b* (**Supplementary Figure 3B**), compensatory to the impaired splicing and function. Before further analysis, we removed outliers using multidimensional scaling plots (**Supplementary Figure 3C**) and excluded samples that differed significantly from the others in the expression of immediate-early stress-responsive genes (**Supplementary Figure 3D**). RNA-seq revealed 1,736 differentially expressed genes in the *Slc7a10b* loss-of-function zebrafish, including 880 upregulated and 856 downregulated transcripts. The loss-of-function caused a particularly striking upregulation of *Urahb* which encodes an enzyme that regulates degradation of uric acid to (S)-allantoin (**Supplementary Figure 4A,B**), a product of purine nucleotide degradation and a marker of oxidative stress in most non-human mammals. Consistently, both urate, purine nucleobase- and hydrogen peroxide metabolism were among the most affected biological processes in the zebrafish VAT, together with, e.g., oxygen transport, AA metabolism,

lipoprotein remodeling, and lipid- and citrate transport (**Supplementary Figure 4B**). The RNA-seq analysis for SLC7A10 inhibition in the differentiating hASCs largely supported an effect on these processes, including steroid biosynthesis and oxidation-reduction process (**Supplementary Figure 5A)**. 121 of the 216 gene ontology terms identified in the zebrafish dataset overlapped with the human dataset. While genes in some terms showed opposite directionality of expression, several of the most significant terms in zebrafish showed the same directionality in human cells (**Supplementary Figure 5A**). . From the 444 differentially expressed genes in the zebrafish dataset, 26 genes overlaped with the human dataset, of which 17 were regulated in the same direction. Among these were *SLC7A10* (reflecting a compensatory up-regulation), *SCD* (a marker of nutritionally regulated lipid storage), *HSD17B10* (an isoleucine catabolizing enzyme), *PKM* and *PC* (related to pyruvate metabolism and glyceroneogenesis which provides glycerol for lipid storage), and *CPT1A* (rate-limiting for mitochondrial lipid β-oxidation) (**Supplementary Figure 5B**).

In accordance with the transcriptome changes indicating effects on mitochondrial function, SLC7A10 inhibition for 24 hours decreased basal respiration, ATP synthesis, maximal consumption rate and spare respiratory capacity by up to 50% in murine (**Supplementary Figure 6A,B**) and primary human adipocytes (**Figure 5A**), with detectable effects after 2-hour inhibition. Exposure to SLC7A10 inhibitor 2 (Lu) reproduced the suppression of maximal consumption rate and spare respiratory capacity (**Figure 5B**). Conversely, overexpressing *Slc7a10* (**Supplementary Figure 6C**) in murine fat cells increased these measures along with basal respiration and ATP synthesis (**Figure 5C**)**.**

SLC7A10 transports serine in adipocytes

To examine the mechanism by which SLC7A10 modulates adipocyte metabolism, we tested the effect of SLC7A10 inhibition on the flux of neutral AAs, some of which are direct precursors of glutathione (e.g., cysteine, glycine and serine) (6,7). SLC7A10 impairment strongly increased medium concentrations of serine from around day 8 of human adipocyte differentiation, while concentrations of other SLC7A10-linked neutral AAs showed only minor effects (**Figure 6A, Supplementary Figure 7A**). We confirmed the reduction in serine influx in response to SLC7A10 inhibition in cultured adipocytes from four independent donors (**Supplementary Figure 7B**).

Additionally, using radiolabeled AAs in sodium-free conditions, SLC7A10-inhibition reduced uptake of D-serine (**Figure 6B and S7C**) and L-serine in adipocytes (**Supplementary Figure 7C,D)**. The primary effect on serine transport is consistent with an important role for this AA in lipid synthesis, antioxidant regeneration, TCA cycle, glycolysis and oxidative phosphorylation, in part because serine serves as a key methyl donor that controls biosynthesis and regeneration of ATP, NADPH, purines, glutathione and other molecules through one-carbon metabolism (11) (**Figure 6C**).

SLC7A10 modulates glutathione levels, ROS generation and insulin-stimulated glucose uptake in adipocytes

The effects of SLC7A10 inhibition on several genes in NADPH- and glutathione-related metabolism (**Figure 6D**) prompted us to examine if SLC7A10 affects cellular glutathione levels. SLC7A10 impairment decreased total glutathione levels detected after only 15-45 minutes inhibition in murine and human adipocytes (**Figure 6E,F**). The decrease was confirmed with inhibitor 2, albeit not significant in the human adipocytes (**Figure 6E,F**), while SLC7A10 overexpression in 3T3-L1 adipocytes increased total glutathione levels (**Figure 6G**). Consistently, intracellular ROS levels increased progressively after 20 minutes of SLC7A10 inhibition in 3T3-L1 adipocytes (**Figure 6H**) and after 60 minutes in mature human adipocytes (**Figure 6I**), while SLC7A10 overexpression reduced ROS generation (**Figure 6J**). Interestingly, when treating SLC7A10-inhibited adipocytes with the ROS scavenger N-acetyl-L-cysteine (Nac), we observed a 50% to 70% reduction in lipid accumulation (**Figure 6K**), indicating that ROS generation may have partially mediated the lipid-storing effect of reduced SLC7A10 activity. On the other hand, this partial reversal of SLC7A10 inhibitor-dependent lipid accumulation by Nac was not clear upon prolonged stimulation with insulin, which increased lipid accumulation to a similar degree as SLC7A10 inhibition (**Figure 6K**). These data suggest that the lipid storing effects of SLC7A10 impairment might at least partially involve increased levels of ROS, whereas the effects of insulin may largely occur independent of ROS generation.

Finally, we tested if reduced SLC7A10 activity also affects insulin-stimulated glucose uptake. Inhibition of SLC7A10 diminished insulin-stimulated glucose uptake in mouse and human

adipocytes (**Figure 7A,B**), supporting that SLC7A10 directly modulates adipocyte insulin sensitivity.

DISCUSSION

We here identified SLC7A10 as a novel facilitator of serine uptake in adipocytes, and that this function may buffer against oxidative stress, lipid accumulation, insulin resistance and dyslipidemia. Our data show that pharmacological inhibition of SLC7A10 in adipocytes decreases glutathione levels (within minutes), increases ROS generation (within an hour), decreases mitochondrial respiratory capacity (within hours) and promotes lipid accumulation (within days). SLC7A10 inhibition also decreases insulin-stimulated glucose uptake. Furthermore, SLC7A10 overexpression showed inverse effects, suggesting that SLC7A10 activation may improve important metabolic functions in adipocytes, potentially counteracting development of obesity and insulin resistance. The overfeeding experiments in zebrafish support that functional impairment of SLC7A10 increases body weight and adipocyte size *in vivo*.

Our clinical cohort data reveal consistent inverse correlations between adipose *SLC7A10* mRNA expression and several key features of insulin resistance, including WHR, adipocyte hypertrophy, visceral fat mass, TAG and HOMA-IR after adjustment for BMI and sex, further underscored by increased *SLC7A10* mRNA in people with insulin sensitive compared to insulin resistant obesity. SC adipose *SLC7A10* was previously shown to have a strong heritable expression (h2 = 0.79), to be lower in people carrying type 2 diabetes risk variants in the *KLF14* locus, and to correlate negatively with metabolic traits linked to disease risk (30).

The potential clinical relevance of SLC7A10 in adipocyte metabolism is further supported by previously unconnected lines of evidence from other studies. Firstly, a metabolomics study found reduced uptake of serine in VAT from people with severe obesity compared to non-obese participants (31) . Secondly, total glutathione levels are higher in OM than SC AT of lean individuals, and altered glutathione synthesis in adipocytes affects insulin sensitivity (32,33). Moreover, total glutathione levels are reduced in AT of people with obesity compared to lean people (34), in line with the pattern of *SLC7A10* expression reported here. Thirdly, SC AT in obesity and type 2 diabetes exhibits increased mitochondrial ROS levels, e.g., hydrogen peroxide (H_2O_2), combined with reduced expression of antioxidant enzymes (35). A recent report showed 46% higher H_2O_2 levels in visceral fat of men with central obesity compared to lean men, and positive correlations of the adipose H_2O_2 concentrations with insulin resistance (36). Importantly,

recent studies suggest that oxidative stress in adipocytes is not only a consequence of metabolic disease, but also a cause (37), and that elevated intracellular ROS levels in adipocytes might contribute to adipocyte dysfunction, increased fat storage and insulin resistance (24,38). Taken together, our study points to SLC7A10 as a potential candidate for therapeutic intervention to mitigate oxidative stress and unhealthy lipid storage in adipocytes.

In line with our experimental data linking reduced SLC7A10 function to increased lipid accumulation via decreased glutathione levels and elevated ROS, glutathione depletion has been found to promote adipogenesis in 3T3-L1 adipocytes (39). Although a recent study in 3T3-L1 adipocytes found that long-term treatment with the ROS scavenger Nac increased ROS levels (40), others found that Nac treatment decreased ROS levels (as expected), while increasing oxygen consumption,decreasing body fat in mice *in vivo* (41) and inhibiting insulin-stimulated lipid accumulation in 3T3-L1 adipocytes (42), in line with our data. ROS can modulate intracellular signaling and a transient increase in ROS levels can promote adipocyte differentiation (38,43), while sustained elevation of cellular ROS levels has been linked to adipocyte lipid storage (24), also observed in microorganisms (44). Our data shows a clear positive relationship between ROS levels and lipid accumulation in contrast to a recent study in mice, where increased mitochondrial levels of the H_2O_2 hydrolyzing enzyme catalase were associated with reduced ROS, increased adiposity,adipocyte size and adipose glyceroneogenic and lipogenic gene expression (45). Another study also found reduced body weight with increased ROS levels in AT with aging (46). A possible explanation for these inconsistent results might be the specific metabolic contexts and distinct effects of specific sources of ROS on glyceroneogenesis and lipid accumulation, which requires further investigation.

It is possible that inhibition of SLC7A10 and the concomitant increase in ROS levels promoted lipid storage in our study, at least in part, by reducing mitochondrial respiratory capacity. A recent study in SC and visceral human adipose-derived stem cells linked high ROS generation to decreased mitochondrial respiration (47), and increased ROS generation in epididymal fat has been shown to precede lowered mitochondrial biogenesis in nutritionally challenged mice (48). Additionally, elevated mitochondrial and extracellular ROS concentrations have been shown to inhibit mitochondrial respiration and to cause mitochondrial dysfunction in cultured 3T3-L1 and

primary rat adipocytes (24,41). Recent studies also showed that ROS can impair insulin-dependent glucose uptake (4,49) in line with the SLC7A10-dependent phenotype we observed .

While our data indicate that altered serine uptake mediated the lipid-storing effects of impaired SLC7A10 function, effects of serine on adipocyte metabolism and mechanisms regulating adipocyte serine flux are largely unknown. Serine is vital in maintaining mitochondrial respiration (50,51) and both imported and *de novo* synthesized serine play a role in protein, lipid and purine metabolism (11). In mouse embryonic fibroblasts lacking the first enzyme in *de novo* serine synthesis, external L-serine depletion increased formation of specific sphingolipids (52) and serine supplementation in mice reduced hepatic ROS levels ameliorating alcoholic fatty liver by supporting glutathione levels (53,54).

Our study has limitations. The SLC7A10 inhibitors BMS-466442 and LU AE00527 have been used to study functions of SLC7A10 in the brain, and show high selectivity (19,20,29,55). However, we cannot entirely rule out nonspecific effects, even though overexpression of SLC7A10 showed inverse effects compared to loss of SLC7A10 function in adipocyte cultures. Previous studies have shown the utility of zebrafish for investigating AT biology and the dynamics of obesity and type 2 diabetes development (56,57), and they share common obesity-related pathophysiological pathways with mammals (58). Nonetheless, future studies should perform adipocyte selective *Slc7a10* manipulation, e.g., by overexpression in mice to determine to what degree maintained Slc7a10 activity can prevent and reverse obesity and systemic insulin resistance. Additionally, further studies are needed to determine whether loss of SLC7A10 activity directly in visceral fat, where *SLC7A10* mRNA is 2-fold higher than in SC fat, might render this depot particularly vulnerable to adipocyte hypertrophy and metabolic dysfunction.

In conclusion, our study has identified *SLC7A10* as a novel gene involved in the regulation of adipocyte energy metabolism, ROS generation and lipid accumulation, implicating novel adipocyte pathways linked to serine transport in obesity and insulin resistance.

ACKNOWLEDGEMENTS

We thank Olivera Bozickovic, Margit Solsvik, Iren Drange Hjellestad and Novin Balafkan at the University of Bergen and Haukeland university hospital, Bergen, Norway and Øyvind Reinshol at the Marine Research Institute (technical assistance), personnel at Voss hospital, Haugesund hospital and Haraldsplass Deaconess hospital, Bergen, Norway (sample collection), and Prof. Per Magne Ueland, University of Bergen, Norway for reviewing the manuscript. We also thank Kenneth Vielsted Christensen at H. Lundbeck A/S for providing the SLC7A10 inhibitor Lu AE00527. This project is supported by the Norwegian Research Council (263124 / F20), Novo Nordisk Scandinavia AS, KG Jebsen Center for Diabetes Research, Western Norway Regional Health Authority and The Norwegian Diabetes Association, Norway. The Genomics Core Facility (GCF) at the University of Bergen, which is part of the NorSeq consortium, provided services on microarray and RNA-seq global gene expression profiling; GCF is supported in part by major grants from the Research Council of Norway (grant no. 245979/F50) and the Trond Mohn Foundation (TMS).

Author Contributions

R.Å.J. and S.N.D. designed the study, carried out experiments analyzed and interpreted the results, and wrote the manuscript. D.S.P.T and A.M. helped carry out experiments, analyze and interpret data and write the manuscript. L.S., L.D., A.W., J-I.B. and M.S.B. assisted with experiments and data analysis. R.Å.J., E.F., L.M. and S.E. performed the zebrafish feeding experiment. A.M. performed metabolomics analyses. V.V., H.N., B.G.N. and C.B. planned and carried out collection of adipose tissue and clinical data. M.B., P.J., P.A.S., M.R., P.A., O.N. and M.C. provided and analyzed cohort data. V.M.S. helped design and support the transcriptome analyses. J.F., J.V.S., G.M. and S.N.D. facilitated the laboratory work, and collection and analyses of cohort samples. All authors reviewed and approved the final version of the manuscript.

Conflict of Interest Statement

The authors declare no competing interests.

Guarantor Statement

S.N.D. is the guarantor of this work and, as such, had full access to all the data in the study and takes responsibility for the integrity of the data and the accuracy of the data analysis.

REFERENCES

1. Acosta JR, Douagi I, Andersson DP, Bäckdahl J, Rydén M, Arner P, et al. Increased fat cell size: a major phenotype of subcutaneous white adipose tissue in non-obese individuals with type 2 diabetes. Diabetologia [Internet]. 2016 Mar 25 [cited 2018 Mar 2];59(3):560–70. Available from: http://www.ncbi.nlm.nih.gov/pubmed/26607638
2. Kim JI, Huh JY, Sohn JH, Choe SS, Lee YS, Lim CY, et al. Lipid-overloaded enlarged adipocytes provoke insulin resistance independent of inflammation. Mol Cell Biol [Internet]. 2015 May [cited 2018 Jul 30];35(10):1686–99. Available from: http://www.ncbi.nlm.nih.gov/pubmed/25733684
3. Heinonen S, Saarinen L, Naukkarinen J, Rodríguez A, Frühbeck G, Hakkarainen A, et al. Adipocyte morphology and implications for metabolic derangements in acquired obesity. Int J Obes [Internet]. 2014 Nov 19 [cited 2018 Jan 31];38(11):1423–31. Available from: http://www.ncbi.nlm.nih.gov/pubmed/24549139
4. Wang C-H, Wang C-C, Huang H-C, Wei Y-H. Mitochondrial dysfunction leads to impairment of insulin sensitivity and adiponectin secretion in adipocytes. FEBS J [Internet]. 2013 Feb [cited 2018 Aug 2];280(4):1039–50. Available from: http://www.ncbi.nlm.nih.gov/pubmed/23253816
5. Szendroedi J, Phielix E, Roden M. The role of mitochondria in insulin resistance and type 2 diabetes mellitus [Internet]. Vol. 8, Nature Reviews Endocrinology. Nat Rev Endocrinol; 2012 [cited 2020 Oct 15]. p. 92–103. Available from: https://pubmed.ncbi.nlm.nih.gov/21912398/
6. Fukasawa Y, Segawa H, Kim JY, Chairoungdua A, Kim DK, Matsuo H, et al. Identification and characterization of a Na(+)-independent neutral amino acid transporter that associates with the 4F2 heavy chain and exhibits substrate selectivity for small neutral D- and L-amino acids. J Biol Chem [Internet]. 2000 Mar 31;275(13):9690–8. Available from: http://www.ncbi.nlm.nih.gov/pubmed/10734121
7. Nakauchi J, Matsuo H, Kim DK, Goto A, Chairoungdua A, Cha SH, et al. Cloning and characterization of a human brain Na(+)-independent transporter for small neutral amino acids that transports D-serine with high affinity. Neurosci Lett [Internet]. 2000 Jun 30;287(3):231–5. Available from: http://www.ncbi.nlm.nih.gov/pubmed/10863037
8. Rosenberg D, Artoul S, Segal AC, Kolodney G, Radzishevsky I, Dikopoltsev E, et al. Neuronal d-Serine and Glycine Release Via the Asc-1 Transporter Regulates NMDA Receptor-Dependent Synaptic Activity. J Neurosci. 2013;33(8).
9. Ussar S, Lee KY, Dankel SN, Boucher J, Haering M-F, Kleinridders A, et al. ASC-1, PAT2, and P2RX5 are cell surface markers for white, beige, and brown adipocytes. Sci Transl Med. 2014;6(247).
10. Yang M, Vousden KH. Serine and one-carbon metabolism in cancer. Nat Rev Cancer [Internet]. 2016 Oct 16 [cited 2018 Sep 16];16(10):650–62. Available from: http://www.ncbi.nlm.nih.gov/pubmed/27634448
11. Newman AC, Maddocks ODK. Serine and Functional Metabolites in Cancer. Trends Cell Biol [Internet]. 2017 Sep 1 [cited 2019 Feb 4];27(9):645–57. Available from: https://www.sciencedirect.com/science/article/pii/S0962892417300752?via%3Dihub

12. Veum VL, Dankel SN, Gjerde J, Nielsen HJ, Solsvik MH, Haugen C, et al. The nuclear receptors NUR77, NURR1 and NOR1 in obesity and during fat loss. Int J Obes [Internet]. 2012 Sep 6 [cited 2018 Sep 21];36(9):1195–202. Available from: http://www.nature.com/articles/ijo2011240

13. Dankel SN, Fadnes DJ, Stavrum A-K, Stansberg C, Holdhus R, Hoang T, et al. Switch from Stress Response to Homeobox Transcription Factors in Adipose Tissue After Profound Fat Loss. Sorensen TIA, editor. PLoS One [Internet]. 2010 Jun 9 [cited 2018 Dec 18];5(6):e11033. Available from: https://dx.plos.org/10.1371/journal.pone.0011033

14. Ahlin S, Sjöholm K, Jacobson P, Andersson-Assarsson JC, Walley A, Tordjman J, et al. Macrophage Gene Expression in Adipose Tissue is Associated with Insulin Sensitivity and Serum Lipid Levels Independent of Obesity. Obesity [Internet]. 2013 Dec [cited 2018 Mar 1];21(12):E571–6. Available from: http://www.ncbi.nlm.nih.gov/pubmed/23512687

15. Saiki A, Olsson M, Jernås M, Gummesson A, McTernan PG, Andersson J, et al. Tenomodulin Is Highly Expressed in Adipose Tissue, Increased in Obesity, and Down-Regulated during Diet-Induced Weight Loss. J Clin Endocrinol Metab [Internet]. 2009 Oct [cited 2018 Mar 1];94(10):3987–94. Available from: http://www.ncbi.nlm.nih.gov/pubmed/19602561

16. Arner E, Mejhert N, Kulyté A, Balwierz PJ, Pachkov M, Cormont M, et al. Adipose tissue MicroRNAs as regulators of CCL2 production in human obesity. Diabetes [Internet]. 2012 Aug 1 [cited 2020 Sep 8];61(8):1986–93. Available from: http://ncbi.nim.nih.gov/geo

17. Lee M-J, Fried SK. Optimal Protocol for the Differentiation and Metabolic Analysis of Human Adipose Stromal Cells. In: Methods in enzymology. 2014. p. 49–65.

18. Dankel SN, Degerud EM, Borkowski K, Fjære E, Midtbø LK, Haugen C, et al. Weight cycling promotes fat gain and altered clock gene expression in adipose tissue in C57BL/6J mice. Am J Physiol Metab. 2014 Jan;306(2):E210–24.

19. Brown JM, Hunihan L, Prack MM, Harden DG, Bronson J, Dzierba CD, et al. In vitro Characterization of a small molecule inhibitor of the alanine serine cysteine transporter -1 (SLC7A10). J Neurochem [Internet]. 2014;129(2):275–83. Available from: http://www.ncbi.nlm.nih.gov/pubmed/24266811

20. Sason H, Billard JM, Smith GP, Safory H, Neame S, Kaplan E, et al. Asc-1 Transporter Regulation of Synaptic Activity via the Tonic Release of d-Serine in the Forebrain. Cereb Cortex [Internet]. 2016 Jan 20 [cited 2016 Nov 15];bhv350. Available from: http://www.ncbi.nlm.nih.gov/pubmed/26796213

21. Mi H, Muruganujan A, Huang X, Ebert D, Mills C, Guo X, et al. Protocol Update for large-scale genome and gene function analysis with the PANTHER classification system (v.14.0). Nat Protoc [Internet]. 2019 Mar 25 [cited 2019 Apr 4];14(3):703–21. Available from: http://www.nature.com/articles/s41596-019-0128-8

22. Midttun Ø, McCann A, Aarseth O, Krokeide M, Kvalheim G, Meyer K, et al. Combined Measurement of 6 Fat-Soluble Vitamins and 26 Water-Soluble Functional Vitamin Markers and Amino Acids in 50 μL of Serum or Plasma by High-Throughput Mass Spectrometry. Anal Chem [Internet]. 2016 Nov 17 [cited 2019 May 13];88(21):10427–36. Available from: http://www.ncbi.nlm.nih.gov/pubmed/27715010

23. Bjune J-I, Dyer L, Røsland G V., Tronstad KJ, Njølstad PR, Sagen J V., et al. The homeobox factor Irx3 maintains adipogenic identity. Metabolism [Internet]. 2019 [cited 2020 Jan 22];154014. Available from: https://www.sciencedirect.com/science/article/pii/S002604951930229X?via%3Dihub

24. Jones IV AR, Meshulam T, Oliveira MF, Burritt N, Corkey BE. Extracellular Redox Regulation of Intracellular Reactive Oxygen Generation, Mitochondrial Function and Lipid Turnover in Cultured Human Adipocytes. López Lluch G, editor. PLoS One [Internet]. 2016 Oct 14 [cited 2018 Jan 31];11(10):e0164011. Available from: http://www.ncbi.nlm.nih.gov/pubmed/27741233

25. Cinti S, Zingaretti MC, Cancello R, Ceresi E, Ferrara P. Morphologic Techniques for the Study of Brown. In: Adipose Tissue Protocols. New Jersey: Humana Press; 2001. p. 021–51.

26. Edgar R. Gene Expression Omnibus: NCBI gene expression and hybridization array data repository. Nucleic Acids Res. 2002 Jan 1;30(1):207–10.

27. Puri V, Ranjit S, Konda S, Nicoloro SMC, Straubhaar J, Chawla A, et al. Cidea is associated with lipid droplets and insulin sensitivity in humans. Proc Natl Acad Sci [Internet]. 2008 Jun 3 [cited 2018 Feb 12];105(22):7833–8. Available from: http://www.ncbi.nlm.nih.gov/pubmed/18509062

28. Klöting N, Fasshauer M, Dietrich A, Kovacs P, Schön MR, Kern M, et al. Insulin-sensitive obesity. Am J Physiol Metab [Internet]. 2010 Sep [cited 2018 Mar 1];299(3):E506–15. Available from: http://www.physiology.org/doi/10.1152/ajpendo.00586.2009

29. Torrecillas IR, Conde-Ceide S, de Lucas AI, García Molina A, Trabanco AA, Lavreysen H, et al. Inhibition of the Alanine-Serine-Cysteine-1 Transporter by BMS-466442. ACS Chem Neurosci [Internet]. 2019 Mar 14 [cited 2019 Mar 22];acschemneuro.9b00019. Available from: http://pubs.acs.org/doi/10.1021/acschemneuro.9b00019

30. Small KS, Hedman ÅK, Grundberg E, Nica AC, Thorleifsson G, Kong A, et al. Identification of an imprinted master trans regulator at the KLF14 locus related to multiple metabolic phenotypes. Nat Genet [Internet]. 2011;43(6):561–4. Available from: http://www.nature.com/doifinder/10.1038/ng.833

31. Hanzu FA, Vinaixa M, Papageorgiou A, Párrizas M, Correig X, Delgado S, et al. Obesity rather than regional fat depots marks the metabolomic pattern of adipose tissue: An untargeted metabolomic approach. Obesity [Internet]. 2014 Mar [cited 2019 Jun 21];22(3):698–704. Available from: http://www.ncbi.nlm.nih.gov/pubmed/23804579

32. Achari AE, Jain SK. l-Cysteine supplementation increases insulin sensitivity mediated by upregulation of GSH and adiponectin in high glucose treated 3T3-L1 adipocytes. Arch Biochem Biophys [Internet]. 2017 Sep 15 [cited 2019 Jun 24];630:54–65. Available from: https://www.sciencedirect.com/science/article/pii/S0003986117301868

33. Kobayashi H, Matsuda M, Fukuhara A, Komuro R, Shimomura I. Dysregulated glutathione metabolism links to impaired insulin action in adipocytes. Am J Physiol Metab [Internet]. 2009 Jun [cited 2019 Jun 24];296(6):E1326–34. Available from: http://www.physiology.org/doi/10.1152/ajpendo.90921.2008

34. Jankovic A, Korac A, Srdic-Galic B, Buzadzic B, Otasevic V, Stancic A, et al. Differences in the redox status of human visceral and subcutaneous adipose tissues – relationships to obesity and metabolic risk. Metabolism [Internet]. 2014 May 1 [cited 2019 Jun 21];63(5):661–71. Available from: https://www.sciencedirect.com/science/article/pii/S0026049514000341

35. Chattopadhyay M, Khemka VK, Chatterjee G, Ganguly A, Mukhopadhyay S, Chakrabarti S. Enhanced ROS production and oxidative damage in subcutaneous white adipose tissue mitochondria in obese and type 2 diabetes subjects. Mol Cell Biochem [Internet]. 2015 Jan 14 [cited 2018 Feb 1];399(1–2):95–103. Available from: http://www.ncbi.nlm.nih.gov/pubmed/25312902

36. Akl MG, Fawzy E, Deif M, Farouk A, Elshorbagy AK. Perturbed adipose tissue hydrogen peroxide metabolism in centrally obese men: Association with insulin resistance. Sun Q, editor. PLoS One [Internet]. 2017 May 18 [cited 2018 Aug 13];12(5):e0177268. Available from: http://dx.plos.org/10.1371/journal.pone.0177268

37. Maslov LN, Naryzhnaya N V., Boshchenko AA, Popov S V., Ivanov V V., Oeltgen PR. Is oxidative stress of adipocytes a cause or a consequence of the metabolic syndrome? J Clin Transl Endocrinol [Internet]. 2019 Mar 1 [cited 2019 Jul 2];15:1–5. Available from: https://www.sciencedirect.com/science/article/pii/S2214623718300711?dgcid=raven_sd_recommender_email

38. Castro JP, Grune T, Speckmann B. The two faces of reactive oxygen species (ROS) in adipocyte function and dysfunction. Biol Chem [Internet]. 2016 Jan 1 [cited 2018 Aug 29];397(8):709–24. Available from: http://www.ncbi.nlm.nih.gov/pubmed/27031218

39. Vigilanza P, Aquilano K, Baldelli S, Rotilio G, Ciriolo MR. Modulation of intracellular glutathione affects adipogenesis in 3T3-L1 cells. J Cell Physiol [Internet]. 2011 Aug [cited 2018 Aug 13];226(8):2016–24. Available from: http://www.ncbi.nlm.nih.gov/pubmed/21520053

40. Peris E, Micallef P, Paul A, Palsdottir V, Enejder A, Bauzá-Thorbrügge M, et al. Antioxidant treatment induces reductive stress associated with mitochondrial dysfunction in adipocytes. J Biol Chem [Internet]. 2019 Feb 15 [cited 2019 May 31];294(7):2340–52. Available from: http://www.jbc.org/content/294/7/2340

41. Wang T, Si Y, Shirihai OS, Si H, Schultz V, Corkey RF, et al. Respiration in Adipocytes is Inhibited by Reactive Oxygen Species. Obesity [Internet]. 2010 Aug 24 [cited 2018 Jan 31];18(8):1493–502. Available from: http://www.ncbi.nlm.nih.gov/pubmed/20035277

42. Kim J-H, Park S-J, Kim B, Choe Y-G, Lee D-S. Insulin-stimulated lipid accumulation is inhibited by ROS-scavenging chemicals, but not by the Drp1 inhibitor Mdivi-1. López Lluch G, editor. PLoS One [Internet]. 2017 Oct 2 [cited 2018 Feb 28];12(10):e0185764. Available from: http://www.ncbi.nlm.nih.gov/pubmed/28968439

43. Tormos KV, Anso E, Hamanaka RB, Eisenbart J, Joseph J, Kalyanaraman B, et al. Mitochondrial Complex III ROS Regulate Adipocyte Differentiation. Cell Metab [Internet]. 2011 Oct 5 [cited 2018 Jan 31];14(4):537–44. Available from: http://www.ncbi.nlm.nih.gov/pubmed/21982713

44. Shi K, Gao Z, Shi T-Q, Song P, Ren L-J, Huang H, et al. Reactive Oxygen Species-

Mediated Cellular Stress Response and Lipid Accumulation in Oleaginous Microorganisms: The State of the Art and Future Perspectives. Front Microbiol [Internet]. 2017 [cited 2018 Apr 9];8:793. Available from: http://www.ncbi.nlm.nih.gov/pubmed/28507542

45. Townsend LK, Weber AJ, Barbeau PA, Holloway GP, Wright DC. Reactive oxygen species-dependent regulation of pyruvate dehydrogenase kinase-4 in white adipose tissue. Am J Physiol Cell Physiol [Internet]. 2020 Jan 1 [cited 2020 Mar 2];318(1):C137–49. Available from: http://www.ncbi.nlm.nih.gov/pubmed/31721616

46. Findeisen HM, Pearson KJ, Gizard F, Zhao Y, Qing H, Jones KL, et al. Oxidative Stress Accumulates in Adipose Tissue during Aging and Inhibits Adipogenesis. Gimble JM, editor. PLoS One [Internet]. 2011 Apr 14 [cited 2018 Apr 17];6(4):e18532. Available from: http://dx.plos.org/10.1371/journal.pone.0018532

47. Sriram S, Yuan C, Chakraborty S, Tay W, Park M, Shabbir A, et al. Oxidative stress mediates depot-specific functional differences of human adipose-derived stem cells. Stem Cell Res Ther [Internet]. 2019 May 21 [cited 2019 Jun 13];10(1):141. Available from: http://www.ncbi.nlm.nih.gov/pubmed/31113471

48. Wang PW, Kuo HM, Huang HT, Chang AY, Weng SW, Tai MH, et al. Biphasic response of mitochondrial biogenesis to oxidative stress in visceral fat of diet-induced obesity mice. Antioxidants Redox Signal [Internet]. 2014 Jun 1 [cited 2020 Aug 12];20(16):2572–88. Available from: https://pubmed.ncbi.nlm.nih.gov/24111683/

49. Liemburg-Apers DC, Willems PHGM, Koopman WJH, Grefte S. Interactions between mitochondrial reactive oxygen species and cellular glucose metabolism. Arch Toxicol [Internet]. 2015 Aug [cited 2019 Jun 13];89(8):1209–26. Available from: http://www.ncbi.nlm.nih.gov/pubmed/26047665

50. Lucas S, Chen G, Aras S, Wang J. Serine catabolism is essential to maintain mitochondrial respiration in mammalian cells. Life Sci Alliance [Internet]. 2018 May 1 [cited 2018 Dec 19];1(2):e201800036. Available from: http://www.life-science-alliance.org/lookup/doi/10.26508/lsa.201800036

51. Gao X, Lee K, Reid MA, Sanderson SM, Qiu C, Li S, et al. Serine Availability Influences Mitochondrial Dynamics and Function through Lipid Metabolism. Cell Rep [Internet]. 2018 Mar 27 [cited 2018 Oct 29];22(13):3507–20. Available from: http://www.ncbi.nlm.nih.gov/pubmed/29590619

52. Esaki K, Sayano T, Sonoda C, Akagi T, Suzuki T, Ogawa T, et al. L-Serine Deficiency Elicits Intracellular Accumulation of Cytotoxic Deoxysphingolipids and Lipid Body Formation. J Biol Chem [Internet]. 2015 Jun 5 [cited 2018 Dec 19];290(23):14595–609. Available from: http://www.jbc.org/lookup/doi/10.1074/jbc.M114.603860

53. Zhou X, He L, Wu C, Zhang Y, Wu X, Yin Y. Serine alleviates oxidative stress via supporting glutathione synthesis and methionine cycle in mice. Mol Nutr Food Res [Internet]. 2017 Nov [cited 2018 Feb 21];61(11):1700262. Available from: http://www.ncbi.nlm.nih.gov/pubmed/28759161

54. Sim W-C, Yin H-Q, Choi H-S, Choi Y-J, Kwak HC, Kim S-K, et al. L-Serine Supplementation Attenuates Alcoholic Fatty Liver by Enhancing Homocysteine

Metabolism in Mice and Rats. J Nutr [Internet]. 2015 Feb 1 [cited 2019 Mar 26];145(2):260–7. Available from: http://www.ncbi.nlm.nih.gov/pubmed/25644346

55. Mikou A, Cabayé A, Goupil A, Bertrand HO, Mothet JP, Acher FC. Asc-1 Transporter (SLC7A10): Homology Models And Molecular Dynamics Insights Into The First Steps Of The Transport Mechanism. Sci Rep. 2020 Dec 1;10(1):1–12.

56. Den Broeder MJ, Kopylova VA, Kamminga LM, Legler J. Zebrafish as a Model to Study the Role of Peroxisome Proliferating-Activated Receptors in Adipogenesis and Obesity. PPAR Res. 2015;2015:1–11.

57. Zang L, Shimada Y, Nishimura N. Development of a Novel Zebrafish Model for Type 2 Diabetes Mellitus. Sci Rep [Internet]. 2017 Dec 3 [cited 2019 May 8];7(1):1461. Available from: http://www.ncbi.nlm.nih.gov/pubmed/28469250

58. Oka T, Nishimura Y, Zang L, Hirano M, Shimada Y, Wang Z, et al. Diet-induced obesity in zebrafish shares common pathophysiological pathways with mammalian obesity. BMC Physiol [Internet]. 2010 [cited 2016 Nov 10];10(1):21. Available from: http://bmcphysiol.biomedcentral.com/articles/10.1186/1472-6793-10-21

TABLES

Table 1. Overview of the analyzed human cohorts.

Cohort and adiposity	n	% male	Age	BMI (kg/m²)	WHR	% T2D	Tissue	Expression	Figure/ Dataset
BPD-Fat									
Obese	12	25	40.4 ± 12.5	51.5 ± 4.9	n/a	42	SC/OM	Illumina	Supplementary Table 4
Post 1 year	12	25	42.2 ± 11.7	32.9 ± 5.6	n/a	0	SC		
SibPair									
Non-Obese/obese	88	47	65.9 ± 6.7	29.3 ± 5.5	0.94 ± 0.08	18	SC	Affymetrix	Supplementary Table 4, 1E
VLCD									
Obese	24	75	48.3 ± 10.4	37.6 ± 4.9	1.02 ± 0.08	29	SC	Affymetrix	1E, S1B
ADIPO									
Obese	12	33	43.1 ± 10.4	43.8 ± 5.4	n/a	17	SC/OM [a]	Illumina	1A, 1C,
Lean	12	42	43.5 ± 12.1	22.8 ± 2.2	0.89 ± 0.06	0	SC [a]	Illumina	Supplementary Table 4
WNOB									
Obese	324	21	40.4 ± 12.5	42.4 ± 5.4	n/a	21	SC/OM	qPCR	1B
Post 1 year	137		42.6 ± 11.8	28.9 ± 5.2	n/a	0	SC	qPCR	
Non-obese	59	82	49.1 ± 16.5	24.7 ± 3.1	n/a	0	SC	qPCR	
ISO									
Obese IR	40	50	51.5 ± 9.7	45.5 ± 1.4	n/a	0	SC/OM	qPCR	1D
Obese IS	40	50	51.4 ± 9.6	45.1 ± 1.8	n/a	0	SC/OM	qPCR	
RIKEN									
Non-Obese/obese	56	0	42.9 ± 12.0	33.1 ± 9.9	0.93 ± 0.08	0	SC [b]	Affymetrix	1E, S1A

[a]*SLC7A10* expression was measured in isolated adipocytes and stromal vascular fraction (SVF)
[b]*SLC7A10* expression was measured in isolated adipocytes
Abbreviations: BMI, body-mass index; WHR, waist-hip ratio; T2D, type 2 diabetes; 1y post-op, one year after bariatric surgery; SC. subcutaneous; OM, omental; IR, insulin resistant; IS

FIGURE LEGENDS

Figure 1. *SLC7A10* mRNA expression is high in visceral adipose tissue, and correlates inversely with obesity and insulin resistance. *SLC7A10* mRNA expression was measured in human visceral (omental, OM) and subcutaneous (SC) adipose samples by microarrays or by qPCR (calculated relative to *HPRT* mRNA).
(**A**) Adipocytes and stromal-vascular fraction (SVF) were isolated from OM and SC adipose tissues of people with severe obesity (n=12) (ADIPO cohort). *SLC7A10* mRNA expression was measured by Illumina microarrays and genes enriched in the adipocyte fraction relative to SVF are shown. Data are presented as median ± IQR.
(**B**) *SLC7A10* mRNA was measured by qPCR in OM and SC adipose tissues collected from people with morbid obesity (BMI ≥ 40 kg/m2, or above 35 kg/m2 with at least one obesity-related health condition) and SC adipose tissue collected one year after profound fat loss following bariatric surgery from the same subjects (Post-WL) (n =101 pairs) Data are presented as mean ± SD.
(**C**) Adipocytes and SVF were isolated from OM and SC adipose tissues of lean people (n=12) and people with severe adiposity (n=12) (ADIPO cohort). *SLC7A10* mRNA expression was measured by Illumina microarrays. Data are presented as mean ± SD.
(**D**) *SLC7A10* mRNA was measured by qPCR in OM and SC adipose tissues in a cohort of 40 insulin-sensitive obese (ISO) and 40 insulin-resistant obese IRO people (ISO cohort), where insulin resistance was measured by hyperinsulinemic-euglycemic clamp. Data are presented as mean ± SD.
(**E**) Correlations of SC adipose tissue *SLC7A10* mRNA with clinical parameters in the RIKEN (n=56), VLCD (n=24) and Sib Pair (n=88) cohorts, calculated as Spearman's rho with and without adjustment. Data are adjusted for BMI and sex for Sib Pair and VLCD cohorts and for BMI for RIKEN cohort. Symbols outlined in bold indicate statistical significance.
(**F**) *SLC7A10* mRNA was measured in OM (n= 88), SC (n=81) and post-WL SC (n= 88) adipose tissues of obese people without diabetes, and in OM (n= 22), SC (n =23) and post-WL SC (n=24) adipose tissues of obese people with diabetes in the WNOB cohort. Data are presented as mean ± SD. OM, omental; SC; subcutaneous; Post-WL- post-weight loss.
*, p<0.05. **, p<0.01. ***, p<0.001.

Figure 2. Loss of SLC7A10 function in zebrafish in vivo causes body weight gain and visceral adipocyte hypertrophy. Four-month-old wildtype (WT) and Slc7a10b loss-of-function mutant male zebrafish were fed 50-100% more than their regular feed for 8 weeks. Body weight and length were recorded at start and end, and weight, length and adipose morphology were assessed after sacrifice. Visceral adipose tissue from three zebrafish housed in same tank during overfeeding was pooled and RNA was isolated.
(**A**) Body weight and length were measured before and after overfeeding of the zebrafish. Data are presented as mean ± SD (WT (n=31) and loss-of-function (n=36)).
(**B-C**) Visceral adipose and liver tissue were fixed, sectioned (5µm) and stained with hematoxylin and eosin for morphological analyses. Adipocyte size was analyzed and quantified using Image J and average adipocyte size was calculated for each section (WT (n=27) and loss-of-function mutant (n=29)). Pictures representative of the group averages are shown.
*, p<0.05. **, p<0.01. ***, p<0.001.

Figure 3. SLC7A10 regulates lipid accumulation in adipocytes. 3T3-L1 preadipocytes were induced to differentiate into mature adipocytes and harvested every second day throughout differentiation. Cultured primary human adipose stromal cells (hASCs) were induced to differentiate into mature adipocytes and harvested every second or fourth day throughout differentiation. Lipid accumulation was measured by Oil-Red-O lipid staining.
(**A-D**) mRNA expression of 3T3-L1 *Slc7a10* was quantified by qPCR, relative to *Rps13* expression (n=3). mRNA expression of *SLC7A10* from hASC cultures was measured by combining the expression profiles of differentiating fat cells from two people were combined (n=2, donors 1 and 2), and quantified relative to *HPRT* mRNA expression. For western blotting, a representative expression profile is shown (n=2 replicates, for both 3T3-L1 and donor 3) and protein expression was calculated relative to HSP90. 20 and 30 µg protein were loaded per well for 3T3-L1 and hASCs respectively, and the following antibodies were used: HSP90 (1:1000, Cell Signaling, cat.no 4874), SLC7A10 (1:500, Santa Cruz Biotechnology, cat.no sc-292032); HRP goat anti-rabbit IgG (1:10000, Thermo Scientific, cat.no 3546); HRP goat anti-mouse IgG (1:7500, BD Biosciences, cat.no 554002). Data are presented as mean ± SD.
(**E-F**) SLC7A10 inhibition throughout differentiation of 3T3-L1s (day 2-8) and hASC cultures (day 3-12) increased lipid accumulation as measured by Oil-Red-O lipid staining. SLC7A10 inhibitors 1 and 2 were used at a final

concentration of 10 μM. Data for 3T3-L1s and representative hASC cultures (n = 4, donors 4, 5, 6 and 7) are shown (n=3-6 replicate wells). Data are presented as mean ± SD.
*, p<0.05. **, p<0.01. ***, p<0.001.

Figure 4. SLC7A10 inhibition strongly affects genes related to energy metabolism in adipocytes.
SLC7A10-associated gene expression patterns were analyzed in mature adipocytes isolated from SC adipose tissue (A) and in cultured primary human adipose stromal cells (hASCs) treated with DMSO or SLC7A10 inhibitor 1 from day 7-8 during adipogenic differentiation (B-C).
(**A**) Mature adipocytes were isolated from biopsies of people with a BMI between 18 and 45 (n=24, ADIPO cohort). Global gene expression was profiled by Illumina microarrays. Genes across the genome that were co- or anti-expressed with *SLC7A10* (Pearson's correlation β > 0.65) were subjected to PANTHER gene ontology analysis. The biological processes most enriched with *SLC7A10*-correlated genes are shown, with indication of enrichment p-values by the color scale.
(**B-C**) hASCs were obtained from abdominal SC adipose tissue (n=6, donors 8-13), differentiated for 8 days and treated with DMSO or SLC7A10 inhibitor 1 for 24 hours from day 7-8. Gene ontology terms were analyzed by PANTHER following RNA-sequencing. Up- and down-regulated pathways are shown here with enrichment visualized on the x-axis, while the number of genes found in each pathway is shown by the size of the circle. Relative gene expression between SLC7A10 inhibitor 1 and DMSO-treated hASCs is depicted for genes in the top up- and down-regulated pathways (C). Data are presented as mean ± SD.
hASC, human adipose stromal cells
*, p<0.05. **, p<0.01. ***, p<0.001.

Figure 5. SLC7A10 stimulates adipocyte mitochondrial respiratory capacity. Human adipose stromal cells (hASCs) and 3T3-L1 preadipocytes were differentiated for 12 and 8 days respectively and treated for 2-24 hours prior to respiration measurements. Oxygen consumption rate (OCR) and respiratory capacity in live adipocytes were measured by the Seahorse XF Cell Mito Stress Test assay. OCR was measured under basal conditions and after sequential addition of the following compounds at indicated final concentrations; oligomycin (3 uM); Carbonyl cyanide 4-(trifluoromethoxy) phenylhydrazone (FCCP) (1.5 uM); rotenone (1 uM) and antimycin A (1 uM). Outliers were removed based on a Whisker Tukey test of the OCR data for each time point in each well, before basal respiration, ATP production, maximal respiration and spare respiratory capacity were calculated according to the manufacturer's protocol. Results are presented as geometric mean ± 95% confidence interval (n=12-44 replicate wells in a 96-well plate).
(**A**) hASCs (donor 14) were differentiated until day 11 and treated with DMSO or SLC7A10 inhibitor 1 for 2 or 24 hours.
(**B**) 3T3-L1 preadipocytes were differentiated until day 8, and treated with DMSO or SLC7A10 inhibitor 2 for 24 hours from day 7-8
(**C**) 3T3-L1 preadipocytes were induced to differentiate and transfected with an expression plasmid encoding Slc7a10 or empty vector on day 2, 4 and 6, before analysis on day 8.
hASC, human adipose stromal cells; OCR, oxygen consumption rate.
*, p<0.05. **, p<0.01. ***, p<0.001.

Figure 6. SLC7A10 regulates serine uptake, glutathione levels and redox state in adipocytes. Human adipose stromal cells **(**hASCs) from SC adipose tissue (n=6) and 3T3-L1 preadipocytes were cultured, differentiated and treated with DMSO or SLC7A10 inhibitors, or transfected with Slc7a10 expression plasmid. Total glutathione (GSH) levels were measured using a GSH probe coupled to a luciferase reaction (E-G). ROS generation was measured by a ROS probe detected by a laser plate reader (H-J) and lipid accumulation was measured by Oil Red O (K). Fluxes of small neutral amino acids in cultured hASCs in response to the selective SLC7A10 inhibitor 1 (10 μM) were assessed by measuring changes in medium concentrations by GC-MS /MS (A) and by radiometric assays (B).
(**A**) Amino acid flux in cultured hASCs throughout adipogenic differentiation were assessed based on the amino acid concentrations in unconditioned medium and change in concentrations upon cell culture during 48-hour periods. Data for the mean of two replicate wells from a representative experiment is shown (donor 4).
(**B**) Cultured hASCs were washed three times in 37 °C sodium free assay buffer 120 mM choline chloride, 25 mM triethylammonium bicarbonate, 1.5 mM KCl, 1.2 mM CaCl2, 1.2 mM MgCl2, 1.2 mM KH2PO4, 10 mM glucose, 10 mM HEPES, 5.5 mM glucose, adjusted to pH 7.4 and sterile filtered), and treated with SLC7A10 inhibitor 1 for 30 minutes. Unlabeled D-serine was added to designated wells (as positive control), before radioactive-labelled (1 μM)

3H-D-serine was added to all wells. Following incubation at 37 °C for 30 minutes, assays were stopped by placing cells on ice and washing three times with ice cold assay buffer. Cells were lysed and loaded in Ultima Gold fluid cartridges (Perkin Elmer) and isotope retention (counts per minute, CPM) in cell lysates was quantified using a Tri-Carb 4910 TR scintillation counter (Perkin Elmer). CPM values were normalized to protein content in corresponding sample using DC protein assay (Bio-rad) (n=4-6, -donor 3). Data are presented as mean ± SD.
(**C**) Summary figure of serine dependent processes and metabolic pathways modified from Newman and Maddocks (11). Serine is important for several metabolic pathways and processes, such as OXPHOS (oxidative phosphorylation) and is also a precursor for biosynthesis of molecules such as methyl groups, purines, and glutathione (GSH).
(**D**) Gene expression measured by RNA-seq showed an enrichment of genes involved in the pentose phosphate shunt, NADPH regeneration and glutathione metabolic processes (n=6 individuals, donors 8-13). Data are presented as mean ± SD.
(**E-F**) 3T3-L1 preadipocytes and hASCs (donor 6) were induced to differentiate to day 8 and day 12, respectively. Total glutathione (GSH) following treatment with DMSO or SLC7A10 inhibitors 1 and 2 (10 μM) for 15 minutes or 24 hours (3T3-L1s) and 45 minutes (hASCs) (n=10-22 replicate wells), by the GSH/GSSG-Glo Assay (Promega) which uses a GSH probe activated by a luciferase reaction. Data are presented as mean ± SD.
(**G**) 3T3-L1 preadipocytes were induced to differentiate and transfected with Slc7a10 expression plasmid or empty vector on every second day of differentiation (days 2, 4 and 6). Total glutathione (GSH) was measured on day 8 as described above (n= 37-39). Data are presented as mean ± SD.
(**H-I**) 3T3-L1 preadipocytes and hASCs (donors 16, 17) were induced to differentiate until day 8 and day 12 respectively and treated with DMSO or SLC7A10 inhibitors 1 and 2 (10 μM) immediately before the assay. ROS generation was measured using the fluorescent probe CM-H2DCFDA (Thermo Fisher). Cells treated without ROS probe served as negative control. The time-course for a representative experiment is shown (donor 17), together with change in ROS generation from start to end (n=11 replicate wells in 96-well plates). Data are presented as mean ± SD.
(**J**) 3T3-L1 preadipocytes were induced to differentiate and Slc7a10 was overexpressed (1μg/ml or 3μg/ml) for 48-hours (day 6-8) using the transfection reagent TransIT-LT1 and additionally cells were treated with DMSO or SLC7A10 inhibitor 1 for 48-hours (day 6-8). ROS generation was measured on day 8 as described above. Change in ROS generation from start to end is shown here (n =). Data are presented as mean ± SD.
(**K**) 3T3-L1 preadipocytes were induced to differentiate and treated with DMSO or SLC7A10 inhibitors 1 and 2 every second day during differentiation from day 2-8 with and without ROS scavenger N-acetyl-L-cysteine (10 mM) (Sigma Aldrich), and with and without insulin (1 μg/ml) from day 4-8. Lipid accumulation was measured by Oil-Red-O lipid staining (n=3). Data are presented as mean ± SD.
GSH, glutathione; hASC, human adipose stromal cells, ROS, reactive oxygen species.
*, p<0.05, **, p<0.01. ***, p<0.001 (comparing DMSO and SLC7A10 inhibitor without ROS scavenger Nac)
§§§, p<0.05 (comparing with/without ROS scavenger Nac)
†, p<0.05, †††, p<0.001 (comparing DMSO and SLC7A10 inhibitor with ROS scavenger Nac)

Figure 7. SLC7A10 inhibition decreases insulin-stimulated glucose uptake. Glucose uptake was assessed by radiometric assay in cultured 3T3-L1 preadipocytes (A) or hASCs (B) induced to differentiate for 8 and 12 days, respectively. 3T3-L1s were treated with DMSO or SLC7A10 inhibitors 1 and 2 (10 μM) for either 24 hours (day 2-8) or from day 2 to 8, and hASCs (donor 7) were treated with DMSO or SLC7A10 inhibitor 1 (10 μM) for 24 hours (day 11-12). Insulin (final concentration 10 nM) was added 30 minutes prior to the assay, and deoxy-D-[14C]-Glucose was added for 30 minutes. Glucose uptake was measured using a scintillation counter (n=6 replicate wells in 12-well plates). Data are presented as mean ± SD.
hASC, human adipose stromal cells.
**, p<0.01. ***, p<0.001.

SUPPLEMENTARY INFORMATION

Supplementary Information includes **seven figures** and **five tables**, and can be found with this article online.

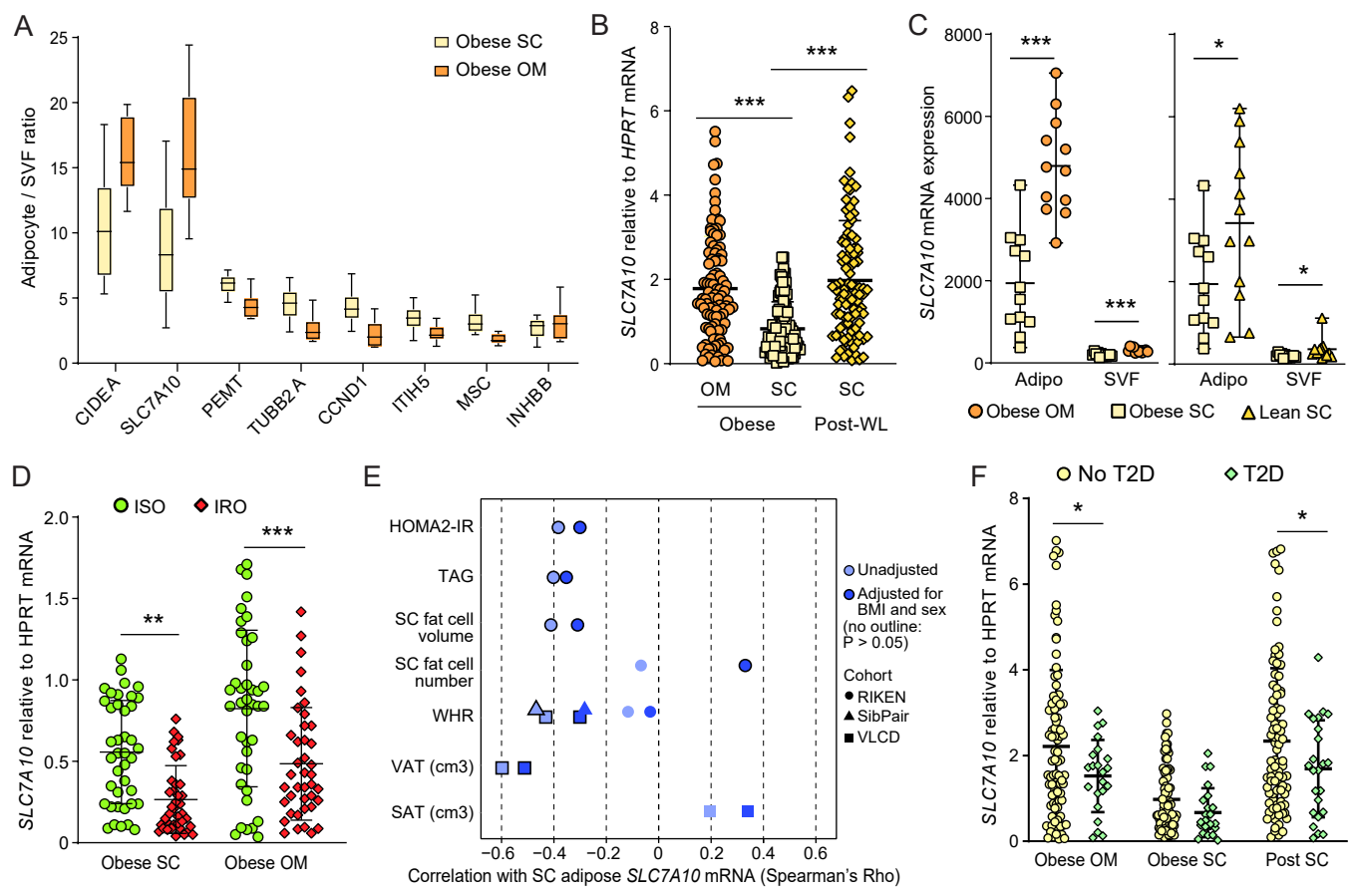
A
Adipocyte / SVF ratio
Obese SC
Obese OM
CIDEA
SLC7A10
PEMT
TUBB2A
CCND1
ITIH5
MSC
INHBB
B
SLC7A10 relative to HPRT mRNA
***
***
OM
SC
SC
Obese
Post-WL
C
SLC7A10 mRNA expression
***
*
***
*
Adipo
SVF
Adipo
SVF
Obese OM
Obese SC
Lean SC
D
ISO
IRO
SLC7A10 relative to HPRT mRNA
**
***
Obese SC
Obese OM
E
HOMA2-IR
TAG
SC fat cell volume
SC fat cell number
WHR
VAT (cm3)
SAT (cm3)
Unadjusted
Adjusted for BMI and sex
(no outline: P > 0.05)
Cohort
RIKEN
SibPair
VLCD
Correlation with SC adipose SLC7A10 mRNA (Spearman's Rho)
F
No T2D
T2D
SLC7A10 relative to HPRT mRNA
*
*
Obese OM
Obese SC
Post SC

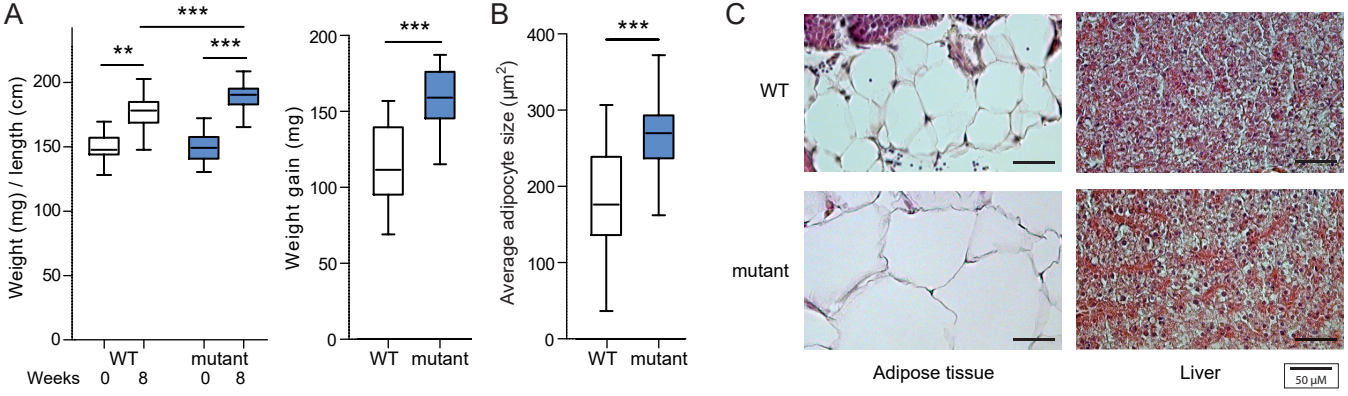
A
Weight (mg) / length (cm)
200
150
100
50
0
**
***
***
WT
mutant
Weeks 0 8 0 8
Weight gain (mg)
200
150
100
50
0
***
WT mutant
B
Average adipocyte size (μm2)
400
300
200
100
0
***
WT mutant
C
WT
mutant
Adipose tissue
Liver
50 μM

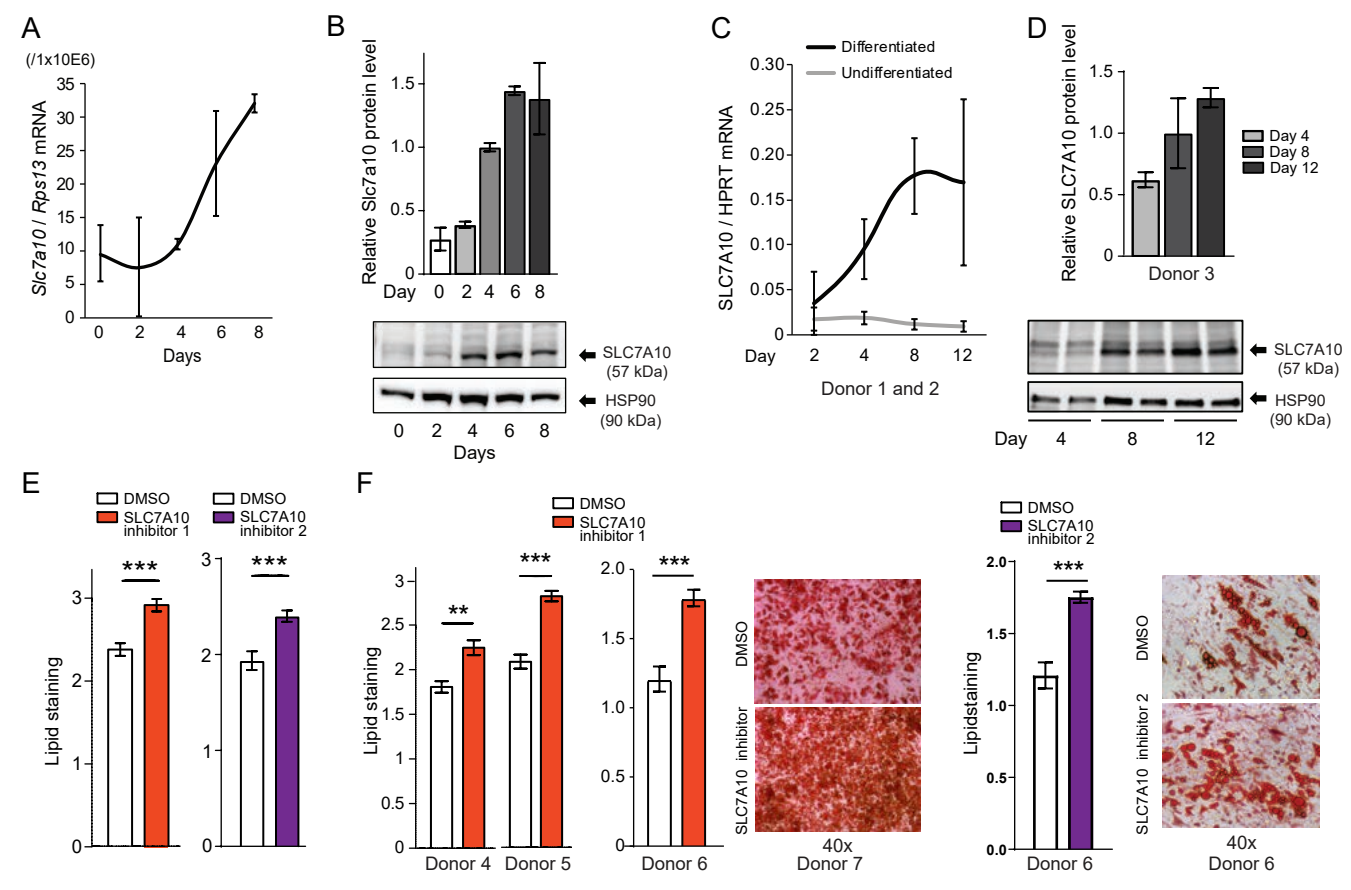
A
(/1x10E6)
Slc7a10 / Rps13 mRNA
Days
B
Relative Slc7a10 protein level
Day 0 2 4 6 8
SLC7A10 (57 kDa)
HSP90 (90 kDa)
Days
C
Differentiated
Undifferentiated
SLC7A10 / HPRT mRNA
Day 2 4 8 12
Donor 1 and 2
D
Relative SLC7A10 protein level
Day 4
Day 8
Day 12
Donor 3
SLC7A10 (57 kDa)
HSP90 (90 kDa)
Day 4 8 12
E
DMSO
SLC7A10 inhibitor 1
DMSO
SLC7A10 inhibitor 2
Lipid staining
***
F
DMSO
SLC7A10 inhibitor 1
Lipid staining
**
***
Donor 4
Donor 5
Donor 6
DMSO
SLC7A10 inhibitor
40x
Donor 7
DMSO
SLC7A10 inhibitor 2
Lipidstaining
Donor 6
DMSO
SLC7A10 inhibitor 2
40x
Donor 6

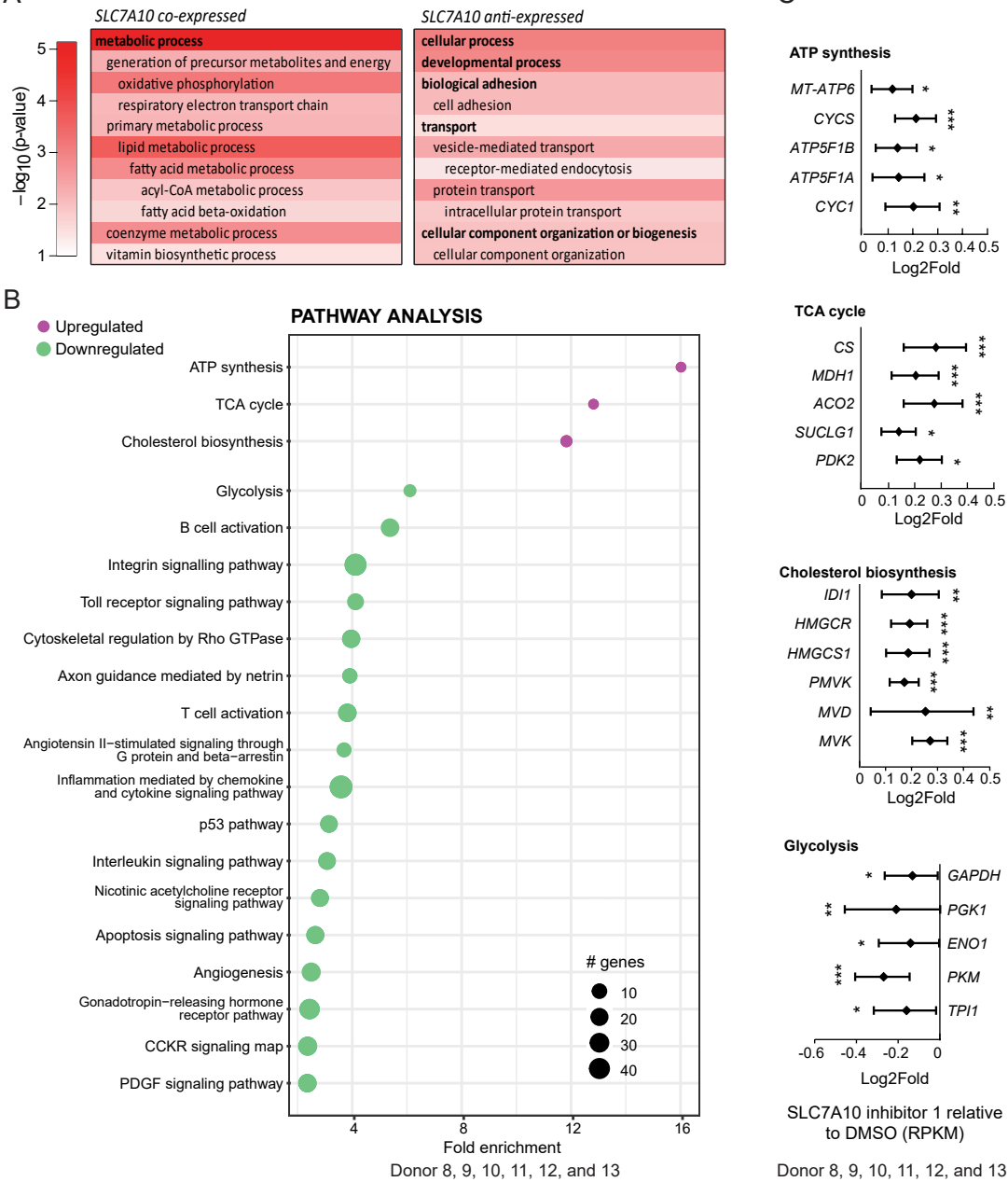
A
SLC7A10 co-expressed
SLC7A10 anti-expressed
− log10 (p-value)
5
4
3
2
1
metabolic process
generation of precursor metabolites and energy
oxidative phosphorylation
respiratory electron transport chain
primary metabolic process
lipid metabolic process
fatty acid metabolic process
acyl-CoA metabolic process
fatty acid beta-oxidation
coenzyme metabolic process
vitamin biosynthetic process
cellular process
developmental process
biological adhesion
cell adhesion
transport
vesicle-mediated transport
receptor-mediated endocytosis
protein transport
intracellular protein transport
cellular component organization or biogenesis
cellular component organization
B
PATHWAY ANALYSIS
Upregulated
Downregulated
ATP synthesis
TCA cycle
Cholesterol biosynthesis
Glycolysis
B cell activation
Integrin signalling pathway
Toll receptor signaling pathway
Cytoskeletal regulation by Rho GTPase
Axon guidance mediated by netrin
T cell activation
Angiotensin II−stimulated signaling through G protein and beta−arrestin
Inflammation mediated by chemokine and cytokine signaling pathway
p53 pathway
Interleukin signaling pathway
Nicotinic acetylcholine receptor signaling pathway
Apoptosis signaling pathway
Angiogenesis
Gonadotropin−releasing hormone receptor pathway
CCKR signaling map
PDGF signaling pathway
genes
10
20
30
40
4
8
12
16
Fold enrichment
Donor 8, 9, 10, 11, 12, and 13
C
ATP synthesis
MT-ATP6
CYCS
ATP5F1B
ATP5F1A
CYC1
0 0.1 0.2 0.3 0.4 0.5
Log2Fold
TCA cycle
CS
MDH1
ACO2
SUCLG1
PDK2
0 0.1 0.2 0.3 0.4 0.5
Log2Fold
Cholesterol biosynthesis
IDI1
HMGCR
HMGCS1
PMVK
MVD
MVK
0 0.1 0.2 0.3 0.4 0.5
Log2Fold
Glycolysis
GAPDH
PGK1
ENO1
PKM
TPI1
-0.6 -0.4 -0.2 0
Log2Fold
SLC7A10 inhibitor 1 relative to DMSO (RPKM)
Donor 8, 9, 10, 11, 12, and 13

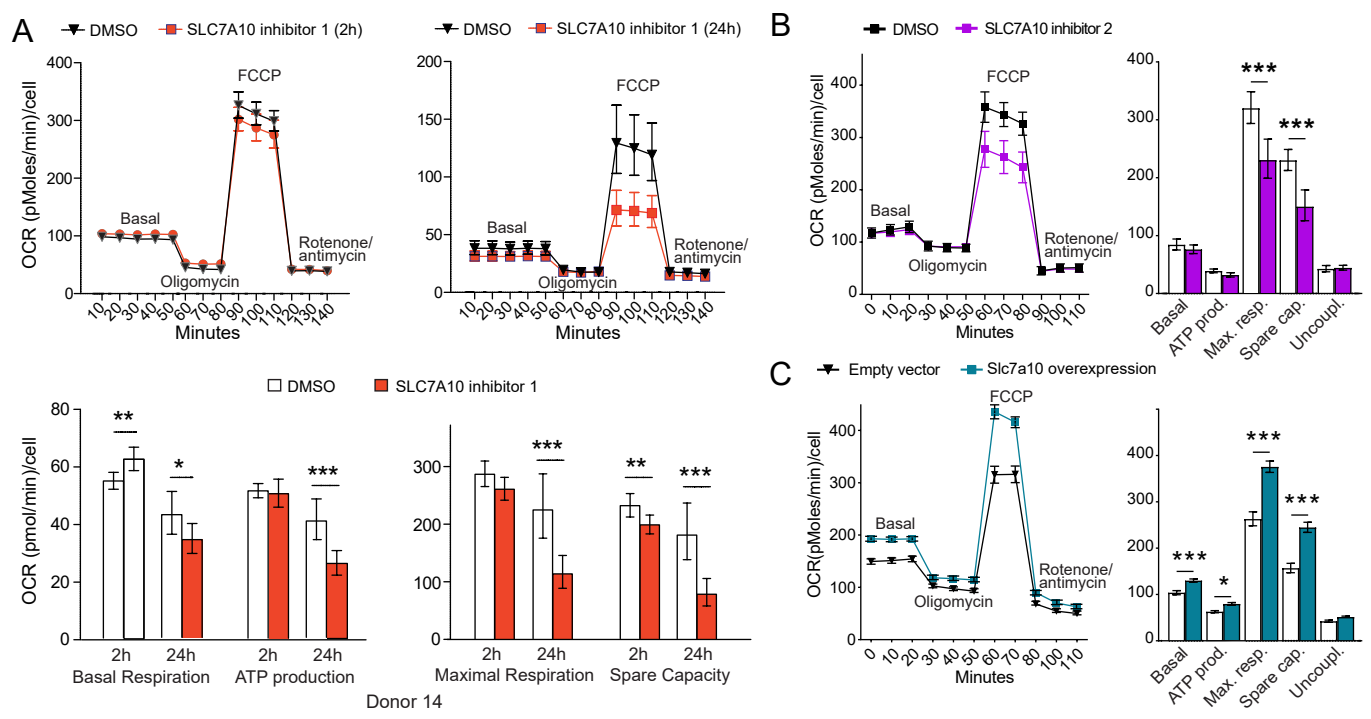
A
DMSO
SLC7A10 inhibitor 1 (2h)
SLC7A10 inhibitor 1 (24h)
OCR (pMoles/min)/cell
FCCP
Basal
Oligomycin
Rotenone/
antimycin
Minutes
B
SLC7A10 inhibitor 2
Basal
ATP prod.
Max. resp.
Spare cap.
Uncoupl.
C
Empty vector
Slc7a10 overexpression
OCR(pMoles/min)/cell
OCR (pmol/min)/cell
SLC7A10 inhibitor 1
2h
24h
Basal Respiration
ATP production
Maximal Respiration
Spare Capacity
Donor 14

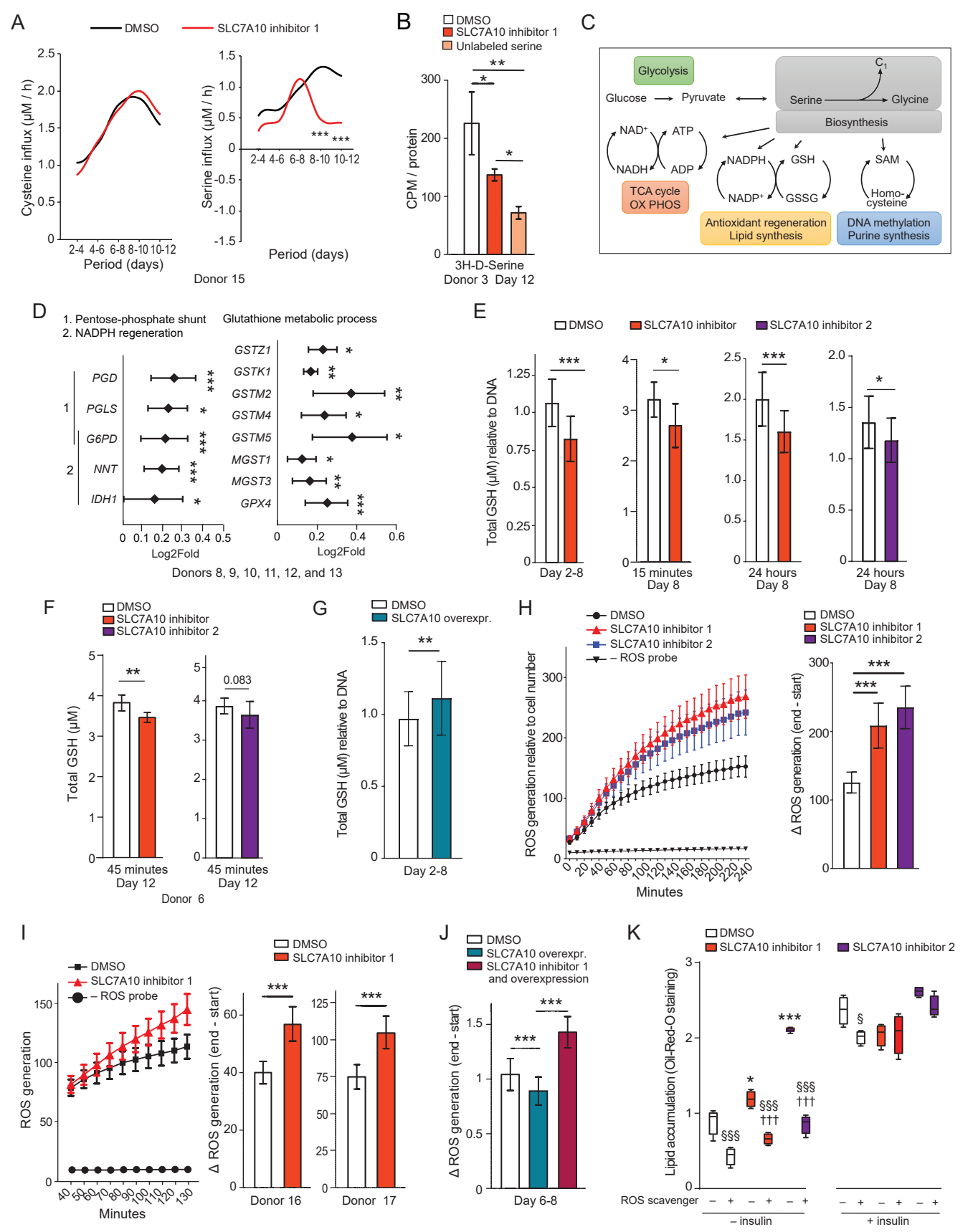
A
DMSO
SLC7A10 inhibitor 1
Cysteine influx (µM / h)
Period (days)
Serine influx (µM / h)
Period (days)
Donor 15
B
DMSO
SLC7A10 inhibitor 1
Unlabeled serine
CPM / protein
3H-D-Serine
Donor 3 Day 12
C
Glycolysis
Glucose
Pyruvate
Serine
Glycine
Biosynthesis
NAD+
NADH
ATP
ADP
NADPH
NADP+
GSH
GSSG
SAM
Homo-cysteine
TCA cycle OX PHOS
Antioxidant regeneration Lipid synthesis
DNA methylation Purine synthesis
D
1. Pentose-phosphate shunt
2. NADPH regeneration
Glutathione metabolic process
PGD
PGLS
G6PD
NNT
IDH1
GSTZ1
GSTK1
GSTM2
GSTM4
GSTM5
MGST1
MGST3
GPX4
Log2Fold
Donors 8, 9, 10, 11, 12, and 13
E
DMSO
SLC7A10 inhibitor
SLC7A10 inhibitor 2
Total GSH (µM) relative to DNA
Day 2-8
15 minutes Day 8
24 hours Day 8
24 hours Day 8
F
DMSO
SLC7A10 inhibitor
SLC7A10 inhibitor 2
Total GSH (µM)
45 minutes Day 12
45 minutes Day 12
Donor 6
G
DMSO
SLC7A10 overexpr.
Total GSH (µM) relative to DNA
Day 2-8
H
DMSO
SLC7A10 inhibitor 1
SLC7A10 inhibitor 2
– ROS probe
ROS generation relative to cell number
Minutes
DMSO
SLC7A10 inhibitor 1
SLC7A10 inhibitor 2
Δ ROS generation (end - start)
I
DMSO
SLC7A10 inhibitor 1
– ROS probe
ROS generation
Minutes
DMSO
SLC7A10 inhibitor 1
Δ ROS generation (end - start)
Donor 16
Donor 17
J
DMSO
SLC7A10 overexpr.
SLC7A10 inhibitor 1 and overexpression
Δ ROS generation (end - start)
Day 6-8
K
DMSO
SLC7A10 inhibitor 1
SLC7A10 inhibitor 2
Lipid accumulation (Oil-Red-O staining)
ROS scavenger
– insulin
+ insulin

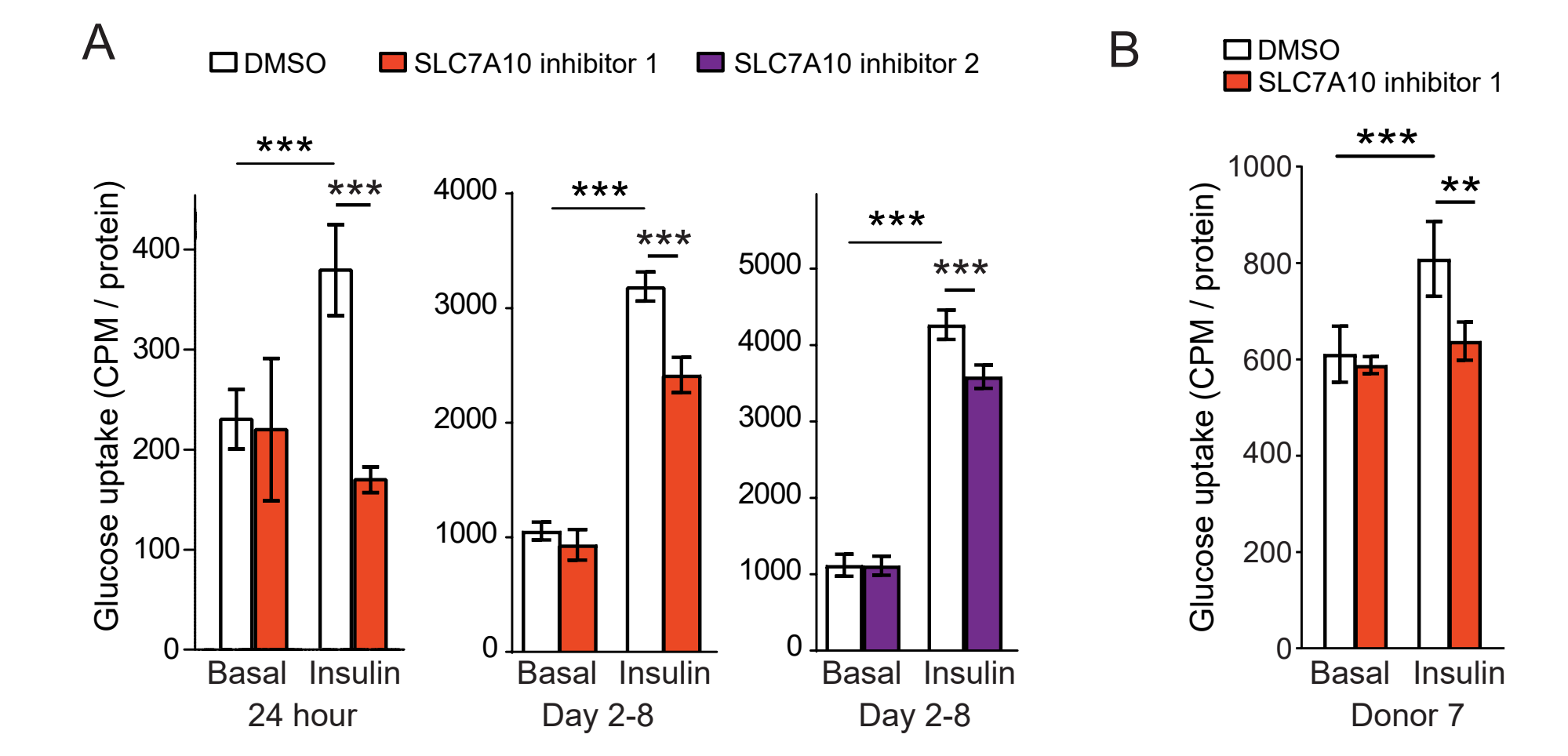
A
DMSO
SLC7A10 inhibitor 1
SLC7A10 inhibitor 2
Glucose uptake (CPM / protein)
***
***
***
***
***
***
Basal
Insulin
24 hour
Day 2-8
Day 2-8
B
DMSO
SLC7A10 inhibitor 1
***
**
Donor 7

SUPPLEMENTARY MATERIAL

Jersin et al. Role of the neutral amino acid transporter SLC7A10 in adipocyte lipid storage, obesity and insulin resistance.

This file includes:

Supplementary Tables:

Supplementary Figures:

Supplementary References

Supplementary Tables

Supplementary Table 1. Primers used for qPCR.

Gene	Forward primer (5' → 3')	Reverse primer (5' → 3')
SLC7A10 Human	CGCCCTCCCCAGTCC	CCCGAGCCGATGATGTTC
*HPRT** Human	TGACCTTGATTTATTTTGCATACC	CGAGCAAGACGTTCAGTCCT
Slc7a10 Mouse	CTTCTGGATGACACCGTCTG	GATGGCACGAGGTAGGTTCT
*Rps13** Mouse	CAGGTCCGTTTTGTGACTG	AGCATCCTTATCCTTTCTGT

* Reference gene

Supplementary Table 2. Characteristics of donors of liposuction material for human primary adipose stromal cell (hASC) cultures.

Donor no.	Figure no.	Age	BMI
1	3C	53	26.4
2	3C	41	32.4
3	3D, 6B	67	26
4	3F, S7B	32	26.9
5	3F, S7B	52	24.3
6	3F, S7C	52	30
7	3F, 6K	52	26.7
8	4B-C, S2A-D, S5A-B, 6D	53	31.5
9*	4B-C, S2A-D, S5A-B, 6D	36	24.3
10	4B-C, S2A-D, S5A-B, 6D	21	29.4
11	4B-C, S2A-D, S5A-B, 6D	58	28
12	4B-C, S2A-D, S5A-B, 6D	45	28.4
13	4B-C, S2A-D, S5A-B, 6D	45	30
14	5A	32	25.5
15	6A, S6A-B	48	27.7
16	6H	46	24.3
17	6H	32	28.4
18	S6B	68	32.8

* Male.

Supplementary Table 3. Plasmids for overexpression.

Vector name	Description	Manufacturer
pCMV6-Kan/Neo	mSlc7a10 (untagged)	Origene
pCMV6-XL4/XL5/XL6	TrueClone™ Empty vector	Origene

Supplementary Table 4. mRNA expression and correlations for identified candidate genes with differential expression in human adipose tissue (Jersin et al. *Diabetes*)

Cohort:		BPD-Fat (n=12)		ADIPO (n=12)						SibPair (n=88)				
		OM/SC	Post/Pre	OM mRNA			SC mRNA			$WHR = \alpha + \beta_1 SEX + \beta_2 BMI + \beta_3 GENE\ EXPRESSION + \varepsilon$				
Symbol	Probe ID	mRNA ratio		Whole	Adipo	SVF	Whole	Adipo	SVF	Probe ID	SC mRNA	R-square*	p-value	pos or neg
Higher in OM vs. SC fat, up-regulated in SC fat after fat loss														
CIDEA	ILMN_2390318	1.70	1.64	1 094	5 627	312	655	2 522	235	221295_at	155	0.520	0.0002	neg
DFNA5	ILMN_1670145	1.77	1.96	920	835	2 344	385	478	1 552	203695_s_at	28.3	0.450	0.122	ns
FLRT2	ILMN_1769615	1.63	1.90	565	255	1 696	313	407	841	204359_at	36.1	0.460	0.048	pos
GAS1	ILMN_2062701	1.73	2.02	1 155	368	2 685	603	256	1 801	204457_s_at	194	0.478	0.010	pos
GPD1L	ILMN_1694106	1.65	1.77	2 049	4 647	2 421	1 193	1 607	1 974	212510_at	95.2	0.590	2.14x10-7	neg
HOXA5	ILMN_1753613	2.38	2.11	1 418	4 692	4 448	800	2 797	2 819	213844_at	50.2	0.469	0.021	neg
SLC7A10	ILMN_1681087	1.83	1.84	1 603	4 986	312	866	2 225	204	220868_s_at	20.5	0.510	0.001	neg
Higher in OM vs. SC fat, down-regulated in SC fat after fat loss														
ALDH1A2	ILMN_1748538	-1.54	2.48	1 686	464	5 459	505	215	814	207016_s_at	18.0	0.498	0.002	pos
GFPT2	ILMN_1709674	-1.93	1.61	1 153	240	1 225	782	243	1 252	205100_at	12.4	0.443	0.247	ns
PDLIM3	ILMN_2230025	-1.55	1.94	989	487	1 478	513	250	676	209621_s_at	7.9	0.448	0.150	ns
TFPI2	ILMN_2068104	-1.52	1.94	577	221	694	269	178	223	209278_s_at	66.8	0.437	0.542	ns
TMEM158	ILMN_1792455	-1.63	1.67	568	285	964	382	304	445	213338_at	2.8	0.472	0.016	pos
Lower in OM vs. SC fat, up-regulated in SC fat after fat loss														
APOC1	ILMN_1789007	3.21	-1.53	309	259	873	544	536	1 556	204416_x_at	50.0	0.445	0.191	ns
COL6A3	ILMN_2307861	1.67	-1.54	3 342	3 154	15 450	5 519	3 276	23 271	201438_at	569	0.447	0.167	ns
CTHRC1	ILMN_2117508	1.52	-2.01	306	154	378	747	180	1122	225681_at	103	0.465	0.029	pos
CTSG	ILMN_1680424	2.41	-1.64	576	181	2 799	1 135	220	7 428	205653_at	14.4	0.515	0.0003	pos
DCLK1	ILMN_2165354	1.98	-1.56	418	396	1 465	696	471	3 725	229800_at	91.2	0.462	0.041	pos
EMX2	ILMN_2187746	1.63	-1.54	151	175	183	239	443	634	221950_at	12.0	0.489	0.003	pos
FNDC1	ILMN_2163873	3.60	-1.62	205	146	299	322	190	2 152	226930_at	13.6	0.443	0.246	ns
PRRX1	ILMN_1739496	1.76	-2.23	1 112	707	4 367	2 266	1 014	11 052	226695_at	202	0.518	0.0002	pos
SERPINA5	ILMN_1759910	1.52	-3.10	165	163	243	559	202	1925	209443_at	12.6	0.468	0.024	pos

Lower in OM vs. SC fat, down-regulated in SC fat after fat loss														
CCND1	ILMN_1688480	-1.62	-3.23	2 587	4 866	3 457	7 409	18 302	4 661	208712_at	124	0.471	0.017	pos
DARC	ILMN_1723684	-1.65	-1.55	2 191	1 169	2 456	3 381	666	3 742	208335_s_at	70.5	0.467	0.025	pos
EGFL6	ILMN_2057479	-5.68	-6.95	351	355	711	3 039	15 392	1 146	219454_at	428	0.461	0.045	pos
GPR56	ILMN_1697228	-2.11	-1.64	868	968	1 455	1 347	624	1 959	212070_at	74.7	0.436	0.563	ns
IFIT3	ILMN_1664543	-1.55	-1.53	214	281	255	321	235	293	229450_at	91.5	0.462	0.040	pos
INHBB	ILMN_1685714	-1.80	-1.53	754	1 584	675	1 205	2 511	940	205258_at	75.5	0.478	0.010	pos
ITIH5	ILMN_1731862	-1.60	-1.67	379	515	230	623	1 088	327	219064_at	457	0.486	0.005	pos
MSC	ILMN_1741404	-2.32	-1.72	341	599	274	578	968	312	209928_s_at	3.3	0.470	0.018	pos
NOTCH3	ILMN_1658926	-1.51	-2.58	480	909	888	1 408	3 183	2 143	203238_s_at	16.5	0.479	0.009	pos
PEMT	ILMN_1745806	-1.51	-2.30	1 129	3 191	798	2 368	10 395	1 665	207621_s_at	138	0.486	0.004	pos
RND3	ILMN_1759513	-3.83	-1.69	2 143	782	1 147	2 996	1 959	1 887	212724_at	83.4	0.469	0.020	pos
SERPINA3	ILMN_1788874	-1.83	-1.66	367	211	624	602	325	1 007	202376_at	4.8	0.457	0.063	ns
SNCG	ILMN_1653161	-2.01	-1.63	566	1 163	327	975	3 253	396	209877_at	18.2	0.440	0.334	ns
SOX7	ILMN_2134056	-3.14	-1.82	495	208	214	764	174	258	228698_at	93.1	0.467	0.024	neg
TNFRSF4	ILMN_2112256	-1.94	-1.55	348	346	470	518	270	541	214228_x_at	6.0	0.454	0.085	ns
TUBB2A	ILMN_2044813	-2.51	-1.82	590	867	325	1 101	2 276	516	204141_at	588	0.492	0.003	pos
UPP1	ILMN_1746837	-2.18	-1.50	1 264	506	772	1 749	640	1 214	203234_at	12.3	0.492	0.003	pos

Adipo, isolated adipocyte fraction; neg, negative correlation; ns, non-significant; OM, omental adipose tissue; pos, positive correlation; Pre, samples obtained before bariatric surgery; Post, samples obtained one year after bariatric surgery; SC, subcutaneous adipose tissue; SVF, stromal vascular fraction; Whole, whole adipose tissue.

Supplementary Table 5. mRNA co-expression with SLC7A10/ASC-1 mRNA in human adipocytes from the ADIPO cohort (12 lean, 12 obese) (Jersin et al. *Diabetes*)

SYMBOL	Coeff.	SYMBOL	Coeff.	SYMBOL	Coeff.	SYMBOL	Coeff.
SLC7A10	*1*	*continued*		*continued*		*continued*	
UTX	*0.909*	CCNH	*0.766*	PHYH	*0.734*	DNAJA3	*0.715*
BCKDHB	*0.895*	PPP1R16A	*0.766*	RAPGEF4	*0.734*	GSDMB	*0.715*
AK3L1	*0.850*	ACOT1	*0.764*	(undefined)	*0.733*	HIBADH	*0.714*
TMEM22	*0.839*	MLYCD	*0.763*	MED26	*0.733*	CD40	*0.714*
RPL34	*0.836*	TP53I13	*0.763*	HIGD2A	*0.733*	TMEM69	*0.713*
LGALS12	*0.830*	UBTD1	*0.760*	C7orf26	*0.733*	LACTB2	*0.713*
BRP44L	*0.826*	CMTM7	*0.760*	ABCC9	*0.732*	MRPL46	*0.713*
COX7C	*0.822*	CCBL2	*0.758*	LOC731007	*0.731*	SOX6	*0.713*
CHL1	*0.822*	FAM73B	*0.758*	POLS	*0.731*	GSDMB	*0.712*
MCCC1	*0.822*	CKB	*0.757*	PIGP	*0.730*	D2HGDH	*0.710*
DHTKD1	*0.821*	MRPS11	*0.756*	C14orf2	*0.730*	FGFRL1	*0.710*
AGT	*0.820*	MOSC2	*0.755*	DTNA	*0.730*	PPP1R1B	*0.710*
SDHB	*0.818*	PCCA	*0.755*	LETMD1	*0.730*	ZFHX4	*0.710*
ACADM	*0.817*	COX5A	*0.755*	TFAM	*0.729*	RHOT1	*0.708*
NDUFB5	*0.812*	RTCD1	*0.755*	MRPS34	*0.729*	(undefined)	*0.708*
MOSC1	*0.808*	CYC1	*0.755*	(undefined)	*0.729*	NAALAD2	*0.708*
COQ9	*0.808*	FLJ23834	*0.754*	CSNK2A1	*0.728*	TXNDC12	*0.707*
C7orf30	*0.803*	AQP7P2	*0.754*	CICE	*0.728*	FABP5	*0.707*
ATL2	*0.802*	RTN3	*0.753*	DTNA	*0.728*	LOC653145	*0.707*
C6orf66	*0.798*	LOC648605	*0.753*	(undefined)	*0.727*	SNX5	*0.706*
C17orf95	*0.795*	ZFPM1	*0.753*	(undefined)	*0.727*	PCBD1	*0.706*
ELOVL3	*0.795*	(undefined)	*0.752*	MRPL21	*0.725*	TSPAN13	*0.706*
VPS54	*0.789*	MCAT	*0.750*	HAX1	*0.724*	ORMDL3	*0.705*
ALDH1L1	*0.789*	LOC652837	*0.749*	CMC1	*0.723*	CNIH	*0.705*
DDT	*0.789*	CAMK1	*0.749*	LOC653479	*0.723*	CCT7	*0.704*
UBE2W	*0.788*	GART	*0.748*	UCKL1	*0.723*	PATL1	*0.703*
UQCRFS1	*0.788*	XRN1	*0.748*	SLC25A4	*0.722*	ARIH1	*0.703*
BTF3L4	*0.784*	THYN1	*0.747*	LDHD	*0.722*	CLPP	*0.703*
ANO6	*0.784*	COX5B	*0.746*	C12orf45	*0.722*	CASD1	*0.702*
RDH10	*0.783*	PXMP2	*0.746*	DMRT2	*0.721*	C4orf14	*0.702*
UQCRH	*0.783*	POLR1D	*0.745*	PXMP2	*0.720*	AUH	*0.701*
LOC646345	*0.780*	LOC648695	*0.745*	SH3GLB1	*0.720*	BCKDHB	*0.701*
C7orf44	*0.780*	AK3L1	*0.743*	C2orf56	*0.719*	RFXANK	*0.701*
PCK1	*0.776*	FAM18B	*0.743*	FAM152B	*0.718*	SCO1	*0.701*
ATP5F1	*0.776*	SLC2A1	*0.742*	PCGF6	*0.718*	LOC650494	*0.701*
HSPD1	*0.775*	HIST1H2BD	*0.742*	CCNF	*0.718*	LOC643300	*0.700*
KIAA1191	*0.773*	C21orf70	*0.741*	EXOSC3	*0.718*	GOT1	*0.700*
ACAD8	*0.772*	AK2	*0.741*	ALKBH1	*0.718*	SYPL1	*0.700*
ESRRA	*0.771*	CDH23	*0.739*	PCBD1	*0.717*	DCI	*0.699*
ABHD3	*0.771*	CYB5A	*0.738*	BPHL	*0.717*	MCCC2	*0.699*
SLC25A5	*0.770*	C21orf33	*0.738*	SLC25A40	*0.716*	ACOT2	*0.699*
MRPL41	*0.770*	CS	*0.737*	ATP1B3	*0.716*	(undefined)	*0.699*
ELK1	*0.769*	ENDOG	*0.737*	FBXO21	*0.715*	STOX1	*0.698*
TMLHE	*0.767*	BCKDHB	*0.736*	MRPS22	*0.715*	FRMD4A	*0.698*
C2orf47	*0.767*	MRPL33	*0.735*	ZNF280D	*0.715*	WDR43	*0.698*
SYMBOL	**Coeff.**	**SYMBOL**	**Coeff.**	**SYMBOL**	**Coeff.**	**SYMBOL**	**Coeff.**

continued		*continued*		*continued*		*continued*	
RPAIN	*0.698*	CALML4	*0.687*	TMCO6	*0.674*	MACROD1	*0.660*
MTFMT	*0.698*	RDH14	*0.687*	SEC24B	*0.674*	CA2	*0.659*
SLC4A4	*0.698*	TAF1L	*0.686*	(undefined)	*0.674*	GTF2IRD1	*0.659*
DTNA	*0.698*	DDX47	*0.685*	PRIM1	*0.674*	C17orf61	*0.658*
ANKRD11	*0.697*	CDKN2C	*0.685*	LETMD1	*0.673*	FBXO46	*0.658*
QPCT	*0.697*	THYN1	*0.684*	GBE1	*0.673*	HSCB	*0.658*
FGFRL1	*0.696*	SDHA	*0.682*	TYSND1	*0.673*	NDUFV2	*0.658*
MRPL39	*0.696*	SNORD100	*0.682*	EBAG9	*0.672*	LOC643466	*0.657*
VPS26B	*0.696*	SUMO2	*0.682*	MRPS23	*0.671*	NDUFB11	*0.656*
KIAA0261	*0.696*	KLF15	*0.682*	TMLHE	*0.671*	MGC70857	*0.656*
GCHFR	*0.695*	HSD17B10	*0.681*	MESP1	*0.671*	(undefined)	*0.656*
C1orf66	*0.695*	GNAQ	*0.681*	CPEB2	*0.671*	NDUFV3	*0.655*
SPTB	*0.695*	CMTM7	*0.681*	MKNK2	*0.670*	PMPCB	*0.655*
STRADB	*0.695*	RABGGTB	*0.681*	(undefined)	*0.670*	(undefined)	*0.655*
VPRBP	*0.694*	GGCT	*0.681*	ALDH6A1	*0.670*	VPS35	*0.655*
PLAGL2	*0.694*	SLC3A2	*0.681*	FBXO28	*0.669*	LPIN1	*0.655*
SLC16A7	*0.694*	CNBP	*0.680*	C2orf56	*0.669*	AASDHPPT	*0.655*
ACADL	*0.694*	RSBN1	*0.680*	AGPAT2	*0.669*	LOC642335	*0.655*
NDUFB6	*0.694*	RBMS2	*0.680*	PPARG	*0.669*	NPC1	*0.654*
CRLS1	*0.694*	SCP2	*0.680*	PIGP	*0.668*	SLC2A4	*0.654*
BDH1	*0.693*	(undefined)	*0.680*	STK35	*0.668*	RAVER1	*0.654*
SPRYD4	*0.693*	LOC284023	*0.679*	MAD2L1BP	*0.668*	DAP3	*0.654*
ACADM	*0.693*	(undefined)	*0.679*	CMTM7	*0.667*	L2HGDH	*0.653*
ACP1	*0.693*	ALKBH1	*0.679*	INTS6	*0.667*	MAZ	*0.653*
NCOR2	*0.693*	ZNF280D	*0.679*	SOSTDC1	*0.666*	FMO5	*0.653*
COX6A1	*0.693*	SCN3A	*0.678*	LIX1L	*0.665*	EIF3M	*0.653*
MRPS2	*0.692*	C17orf95	*0.678*	PIK3CB	*0.665*	SEC11A	*0.653*
C9orf72	*0.692*	(undefined)	*0.678*	CS	*0.664*	(undefined)	*0.653*
GFPT1	*0.692*	CNIH	*0.678*	AQP7	*0.664*	PCNX	*0.652*
MLX	*0.692*	CA2	*0.678*	ANKRD9	*0.664*	YPEL5	*0.652*
SNURF	*0.692*	SEPHS1	*0.678*	PDZD7	*0.664*	NDFIP2	*0.652*
BLOC1S1	*0.691*	ESRRAP2	*0.677*	ATAD2	*0.663*	NAT5	*0.652*
PAXIP1	*0.691*	LOC729317	*0.677*	SFXN2	*0.663*	(undefined)	*0.652*
UTP18	*0.691*	(undefined)	*0.677*	MEIS2	*0.663*	HYLS1	*0.652*
C18orf8	*0.690*	NET1	*0.677*	GTPBP3	*0.663*	RPL35A	*0.652*
GLRX2	*0.690*	MCM7	*0.677*	RAB40C	*0.663*	STOX1	*0.651*
LOC652545	*0.690*	DUSP4	*0.677*	TBP	*0.663*	STAMBP	*0.651*
GRPEL1	*0.690*	ICAM3	*0.676*	CLK2	*0.663*	DHPS	*0.651*
CCNC	*0.689*	DNAH1	*0.676*	SEC24B	*0.662*	STBD1	*0.650*
TRPT1	*0.689*	CSNK2A2	*0.676*	NDUFAF2	*0.662*	FBXO44	*0.650*
PATZ1	*0.689*	LOC285074	*0.676*	HINT3	*0.662*	OXA1L	*0.650*
SLC25A22	*0.689*	C16orf14	*0.676*	LOC645436	*0.662*	(undefined)	*0.650*
PC	*0.689*	RPL9	*0.675*	PPP2R2D	*0.662*	ACY1	*0.650*
SMARCD1	*0.688*	(undefined)	*0.675*	(undefined)	*0.661*		
UBQLN1	*0.688*	KIAA0367	*0.675*	PLCXD1	*0.660*		
CASZ1	*0.688*	C1QL2	*0.675*	TCF12	*0.660*		
LDLRAD1	*0.688*	PCCB	*0.675*	ZNF512B	*0.660*		
CXorf15	*0.687*	POLE	*0.674*	MIA3	*0.660*		
	Coeff.	**SYMBOL**	**Coeff.**	**SYMBOL**	**Coeff.**	**SYMBOL**	**Coeff.**

SYMBOL							
(undefined)	*-0.650*	*continued*		*continued*		*continued*	
IFT57	*-0.651*	CANX	*-0.676*	SETBP1	*-0.703*	TLN1	*-0.769*
OLFML1	*-0.651*	ITGA11	*-0.676*	DAB2	*-0.704*	CCNYL1	*-0.769*
TFPI	*-0.652*	CPD	*-0.677*	ZYX	*-0.705*	RAP2A	*-0.771*
C5orf5	*-0.652*	LAPTM5	*-0.677*	SOX4	*-0.705*	FBLN2	*-0.775*
ST5	*-0.653*	ANXA11	*-0.677*	EMX2	*-0.705*	RUFY3	*-0.781*
COL6A2	*-0.653*	FAM129A	*-0.677*	C21orf51	*-0.705*	TMSB10	*-0.786*
CCDC25	*-0.654*	AP1S2	*-0.677*	ACTG1	*-0.707*	IQSEC2	*-0.787*
HABP4	*-0.655*	THBS2	*-0.678*	ZNF219	*-0.709*	PTTG2	*-0.793*
CILP	*-0.655*	ARHGAP28	*-0.678*	COL4A5	*-0.711*	MGP	*-0.845*
LOC648470	*-0.655*	FBLN5	*-0.678*	PDLIM7	*-0.711*	RANBP3L	*-0.846*
PDCL3	*-0.657*	SLC7A2	*-0.679*	RNASEL	*-0.711*		
(undefined)	*-0.657*	MYO1B	*-0.680*	MAP1B	*-0.713*		
KIAA1160	*-0.657*	C1orf24	*-0.681*	STX2	*-0.714*		
KCTD12	*-0.658*	MTTP	*-0.681*	PSAP	*-0.716*		
LOC651302	*-0.659*	SPARC	*-0.681*	ANKS1B	*-0.717*		
TMEM119	*-0.659*	CALM3	*-0.684*	DKK3	*-0.719*		
LUM	*-0.660*	CDH11	*-0.684*	RCN1	*-0.720*		
ITIH5	*-0.661*	ACTB	*-0.685*	SPON2	*-0.723*		
TRPV2	*-0.661*	CAPZB	*-0.685*	DGKI	*-0.724*		
LOC390956	*-0.661*	(undefined)	*-0.685*	CAPNS1	*-0.726*		
CLN5	*-0.662*	LOC389958	*-0.686*	SLC2A12	*-0.726*		
ACTN4	*-0.662*	REEP5	*-0.688*	SAP18	*-0.727*		
(undefined)	*-0.663*	CCDC105	*-0.688*	RNASEL	*-0.732*		
LMOD1	*-0.663*	ACTB	*-0.689*	LOX	*-0.735*		
IFITM5	*-0.663*	DAAM2	*-0.689*	MYO1D	*-0.738*		
(undefined)	*-0.663*	SLC39A3	*-0.689*	SH3BGRL2	*-0.741*		
(undefined)	*-0.664*	CCBP2	*-0.690*	CDC26	*-0.741*		
FLJ22374	*-0.665*	ARHGAP21	*-0.691*	MED20	*-0.742*		
BICD2	*-0.666*	VWA1	*-0.693*	KIAA1598	*-0.742*		
NEXN	*-0.666*	COL4A5	*-0.694*	TAX1BP3	*-0.743*		
CLEC3B	*-0.668*	LPAR1	*-0.694*	DPT	*-0.748*		
(undefined)	*-0.668*	CNN3	*-0.696*	TMEM98	*-0.748*		
SRI	*-0.669*	INHBB	*-0.698*	MGP	*-0.749*		
PON2	*-0.669*	DCTN1	*-0.699*	EMX2	*-0.751*		
CYLN2	*-0.671*	CXCL12	*-0.700*	ABHD4	*-0.754*		
CETN2	*-0.673*	CCND2	*-0.701*	DRAM	*-0.756*		
LOC391013	*-0.673*	PFKP	*-0.701*	ITGA11	*-0.757*		
CANX	*-0.675*	CAMK1D	*-0.702*	(undefined)	*-0.766*		
ITGB5	*-0.675*	ASCC3	*-0.702*	ITGB1	*-0.768*		

Coeff., Pearson's correlation coefficient; SYMBOL, Gene name.

Supplementary Figures

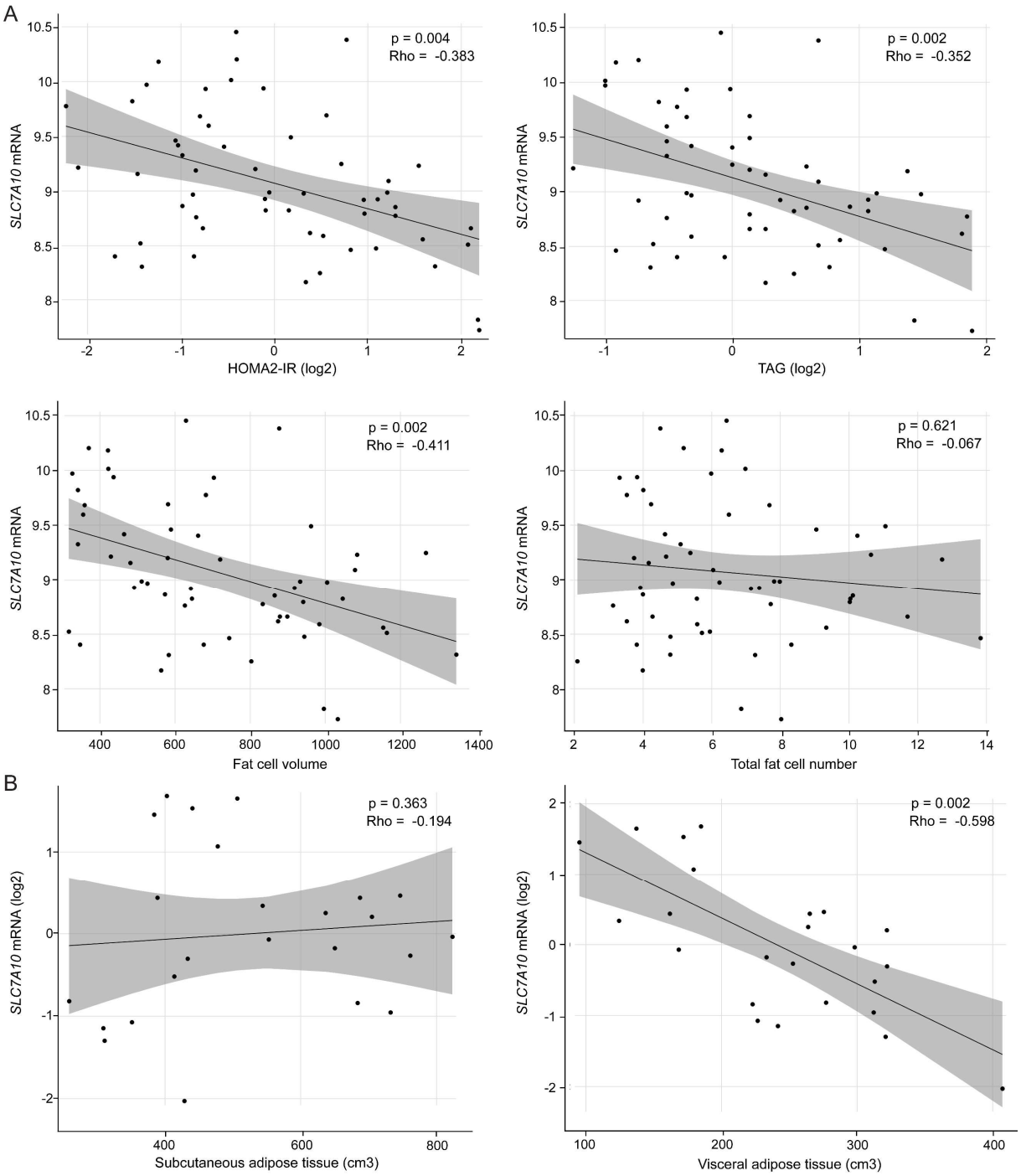

Supplementary Figure 1. Correlations of *SLC7A10* mRNA expression with insulin resistance and adiposity traits in the RIKEN (n=58, panel A) and Sib Pair-Subgroup (n=24, panel B) cohorts.
SLC7A10 mRNA expression was retrieved from microarray expression analyses (Affymetrix) and Spearman correlations were calculated.

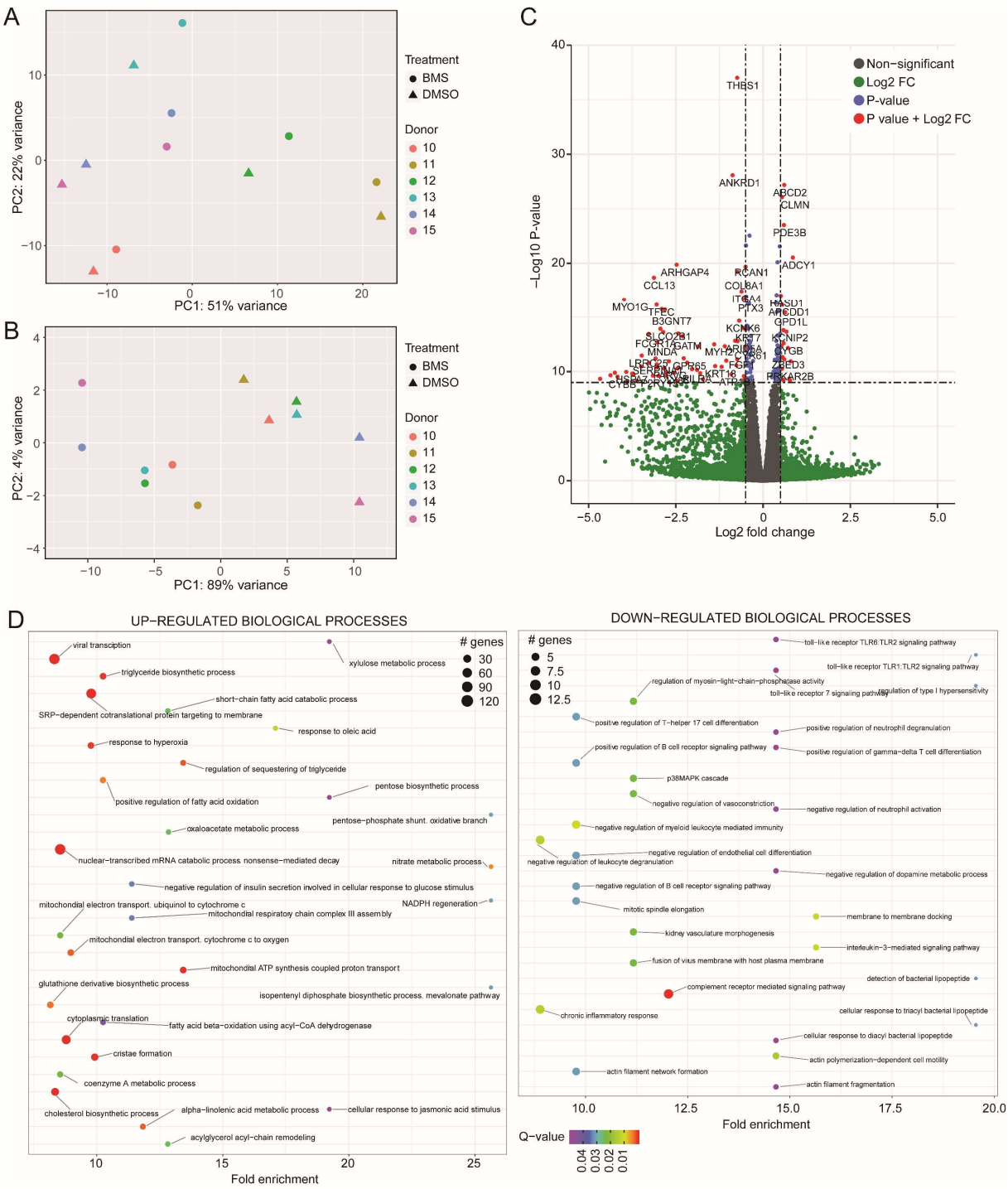

Supplementary Figure 2. Effects of SLC7A10 inhibition on global gene expression measured by RNA-sequencing in human primary adipocytes.
Human adipose stromal cell (hASC) cultures were obtained from abdominal subcutaneous adipose tissue (n=6), differentiated for 8 days, and treated with DMSO or SLC7A10 inhibitor 1 for 24 hours from day 7-8. Global gene expression was measured by RNA-seq, where sample reads were mapped against the Human genome (GrCH38) using HiSat (Version 2.1.0), with options –t "exon" and –g "gene_id" to summarize count values from individual exons into genes, resulting in a matrix of raw counts. Aligned reads were then put into featureCounts (Version 1.5.2) with default options, resulting in a matrix of raw counts. Data were normalized and differential expression analysis was performed utilizing DESeq2 (Version 1.22.2). Pathway analysis of RNA sequencing data was performed using PANTHER classification system (PANTHER v.14.0). Differentially expressed genes identified with a FDR cut-off ($p<0.05$) were used as input and Fischer's exact test was used to identify statistically over/under represented pathways with a FDR cut-off ($p<0.05$) (1). Significant ontologies were visualized using ggplot2 package (Version 3.1.0).

(**A-B**) Principal component (PC) analysis of samples in DMSO and SLC7A10 inhibitor 1 treated groups are shown in (A) unadjusted and (B) adjusted for patient.

(**C**) Volcano plot of differentially expressed genes between DMSO and SLC7A10 inhibitor 1 treatments. x-axis corresponds to log2 fold change (log2FC) and y-axis corresponds to -log10 (P-value). Red dots represent the transcripts with an absolute log2FC > 0.5 and P-value < 10E-10; green dots represent the transcripts with an absolute log2FC > 0.5; blue dots represent transcripts with P-value < 10E-10; grey dots represent transcripts which do not pass above thresholds.

(**D**) Enrichment plot representing up-regulated and down-regulated biological processes between DMSO and SLC7A10 inhibitor treatments. Top 30 biological processes with an FDR-corrected P-value < 0.05 and fold enrichment ≥ 8 (arbitrary threshold for the sake of visual representation) are reported here. Gene Ontology (GO) terms was analyzed by PANTHER (www.pantherdb.org).

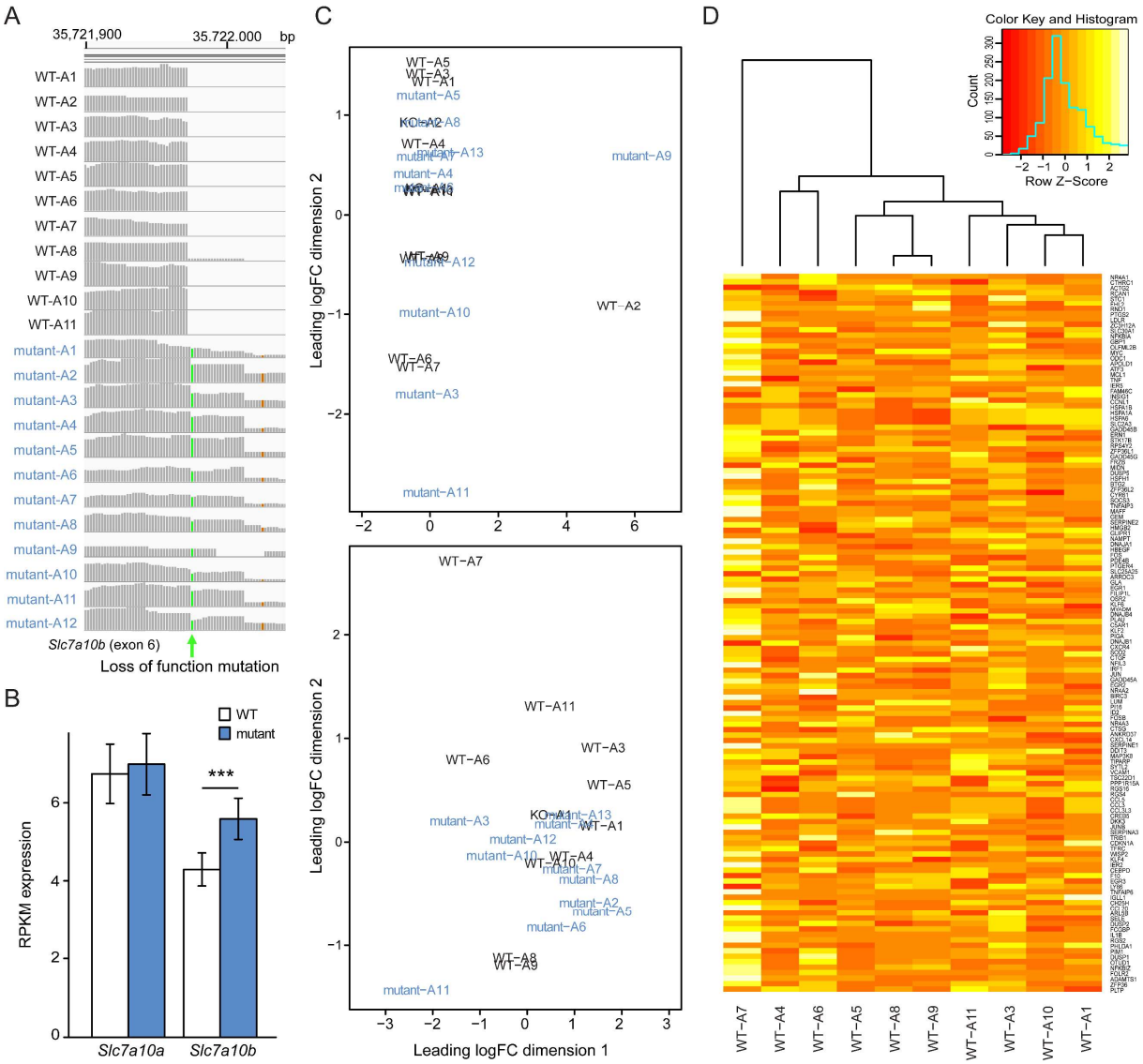

Supplementary Figure 3. Confirmation of Slc7a10b loss-of-function mutation and outlier detection by RNA-sequencing of zebrafish visceral adipose tissue.
Mature (four-month old) wildtype (WT) and Slc7a10b mutant male zebrafish were fed 50-100% more than their regular feed for eight weeks. Visceral adipose tissue from three zebrafish housed in the same tank during the overfeeding was pooled. RNA was isolated and RNA-seq was performed. Sample reads were mapped against the

Zebrafish genome (GRCz10) using HiSat (Version 2.05), matrixed in featureCounts (Version 1.5.2) and analyzed using DESeq2 (version 1.22.1).

(**A**) Integrative genomics viewer (IGV) read visualization of each Zebrafish sample at the target site, with the A→T splice site mutation sa15382 highlighted in green.

(**B**) Visualized expression values (RPKM) of average *Slc7a10a* and *Slc7a10b* expression in both WTs and mutants.

(**C**) Outlier removal of anomalous RNA-Seq sequence reads (by sample) was performed by generating multidimensional scaling plots of distances between digital gene expression profiles. The samples mutant-A9 and WT-A2 were visually identified in the top graph as being erroneous due to their spread from the main cluster in the first dimension. The lower graph displays the distances after the removal of the first two outliers, showing WT-A7 spreading from the main cluster.

(**D**) The differential expression in WT-A7 was further investigated by utilizing the ontology gene expression profiles of the WT samples, and we observed that this sample differed significantly from other wild-types in the expression profile of stress-induced genes identified in human adipose tissue, warranting removal of WT-A7 from further downstream analysis. The stress-induced genes were identified by microarray analysis of omental human adipose tissue biopsies of non-obese patients. Omental biopsies from four patients were either frozen immediately or ~1 hour after surgical excision. The 1-hour delayed freezing induced a large array of immediate-early stress-responsive genes including IL8 (induced already after 10 minutes) [24], largely recapitulating differences we previously observed between lean and extremely obese patients [153] (data not shown). We concluded that the WT-A7 sample was acutely stressed either *in vivo* or *ex vivo*, and that its inclusion in our initial analysis was entirely responsible for an apparent down-regulation of stress-responsive/inflammatory genes in the mutant compared to WT zebrafish. WT-A7 was therefore removed from further analysis, to avoid a dominating artefactual impact on gene ontology terms.

***, $p<0.001$.

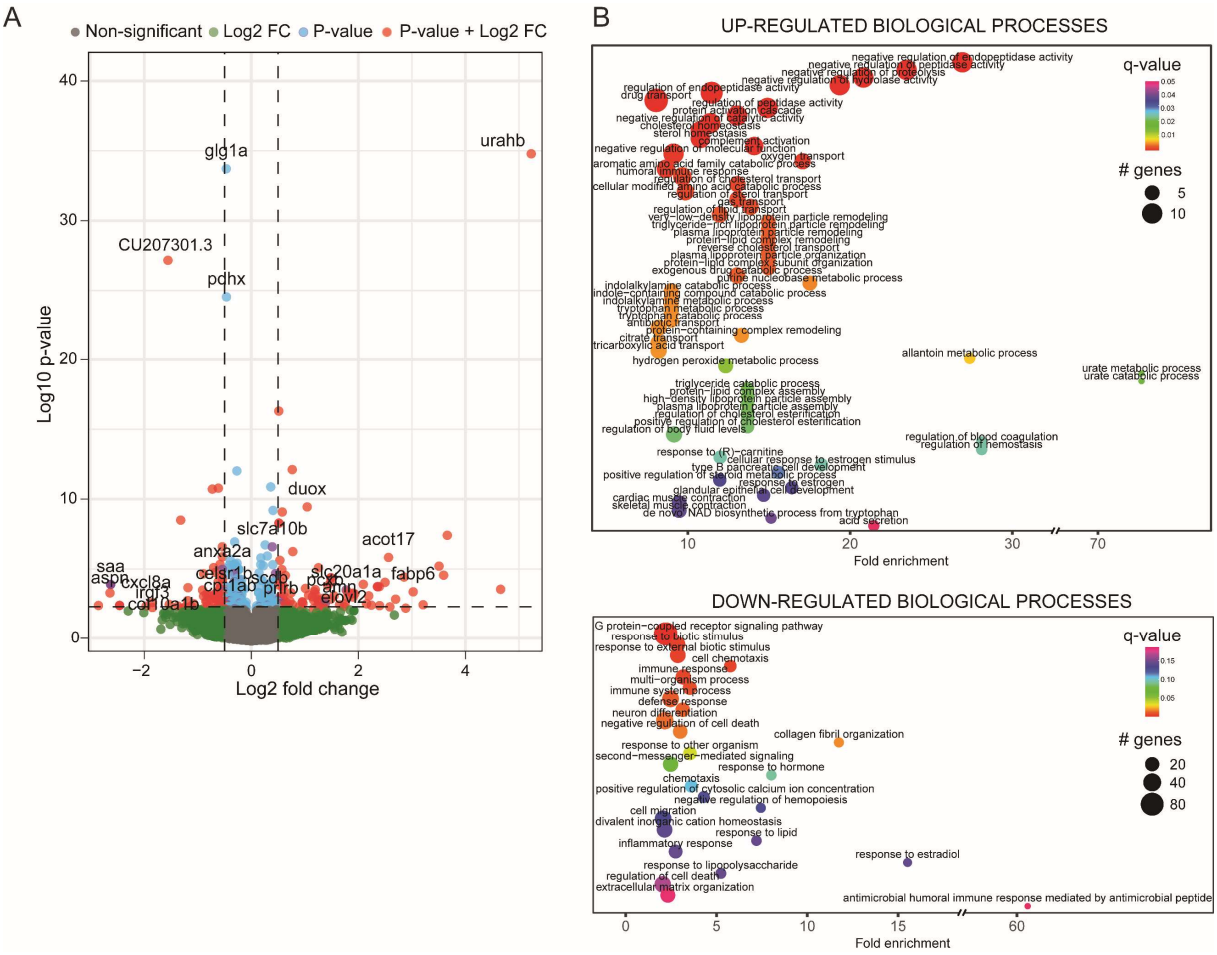

Supplementary Figure 4. Slc7A10b loss-of-function mutation in overfed zebrafish upregulates genes involved in urate, purine, and lipid metabolic processes.
Mature (four-month old) wildtype (WT) and Slc7a10b loss-of-function male zebrafish were fed 50-100% more than their regular feed for eight weeks. Visceral adipose tissue from three zebrafish housed in the same tank during the overfeeding was pooled. RNA was isolated and RNA-seq was performed. Sample reads were mapped against the Zebrafish genome (GRCz10) using HiSat (Version 2.05), matrixed in featureCounts (Version 1.5.2) and analyzed using DESeq2 (version 1.22.1).

(A) Volcano plot of differentially expressed genes between WT and Slc7a10b loss-of-function zebrafish. x-axis corresponds to log2 fold change (log2FC) and y-axis corresponds to -log10 (P-value). The red dots represent the transcripts with an absolute log2FC > 0.5 and P-value < 10E-10; green dots represent the transcripts with an absolute log2FC > 0.5; blue dots represent transcripts with P-value < 10E-10; grey dots represent transcripts which do not pass above thresholds.

(B) Combined differentially expressed genes between Slc7a10b zebrafish WT and mutant into a single ranked list based on fold change, and gene ontology (GO) terms were analyzed using GOrilla (2). Enrichment plot representing up-regulated biological processes between WT and Slc7a10b loss-of-function zebrafish was visualized using the R package ggplot2. Biological processes with a P-value < 0.05 and fold enrichment ≥ 8 (arbitrary threshold for the sake of visual representation) are reported here.

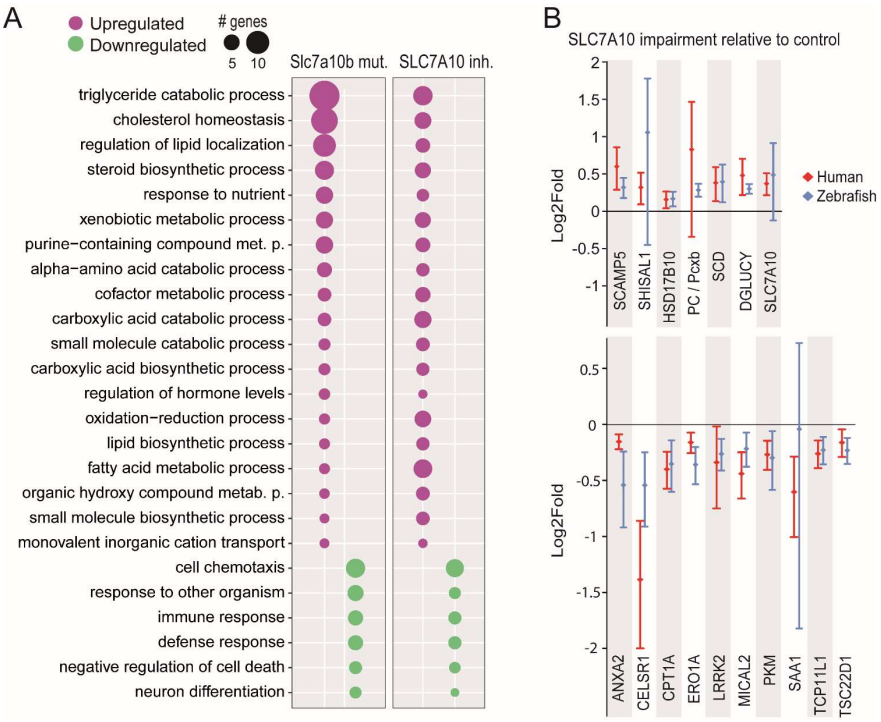

Supplementary Figure 5. SLC7A10 impairment affects genes related to lipid- and energy metabolism in zebrafish adipose tissue and human primary adipocyte cultures.
RNA-sequencing was performed as described in Supplementary Figures 2 and 4. For each dataset, genes were sorted based on fold change into a single ranked list, and analyzed using GOrilla to identify enriched ontologies (2). Significant ontologies were summarized for plotting utilizing the REViGO web package, which clusters representative ontologies via semantic similarity (3). RPKM values for gene expression visualizations were generated using edgeR (Version 3.16.5). Overlapping ontologies between zebrafish adipose tissue and human adipose cultures were plotted using ggplot2 (Version 3.1.0).

(**A**) Gene ontologies enriched with differentially expressed genes identified in RNA-seq from both zebrafish mutant and SLC7A10 inhibitor treated human adipocytes compared to control. Differentially expressed genes were combined into a single ranked list based on fold change using GOrilla analysis (2). Enriched ontologies in both the zebrafish mutant and SLC7A10 inhibitor 1 RNA-seq were aggregated, filtered by enrichment and significance, and plotted by relative enrichment. Overlapping ontologies between Zebrafish and SLC7A10 inhibitor 1 RNA-seq were visualized using the R package ggplot2 (Version 3.1.0).

(**B**) Fold changes for up- and down-regulated genes in RNA-seq from both zebrafish mutant and SLC7A10 inhibitor 1 treated (10 µM) human adipocytes compared to control. Outliers were removed using Whiskers Tukey outlier test. Data are presented as mean ± SD.

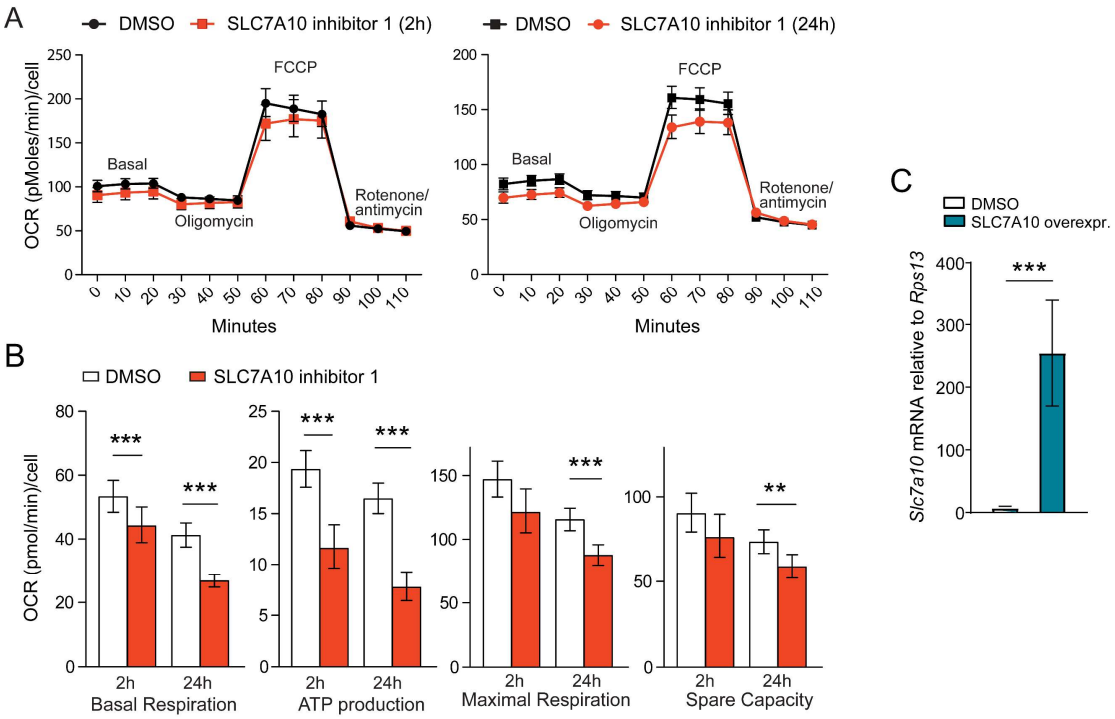

Supplementary Figure 6. SLC7A10 inhibition affects mitochondrial respiration in cultured mouse adipocytes.
3T3-L1s were differentiated and treated with SLC7A10 inhibitor 1 for either 2 or 24 hours, or Slc7a10 was overexpressed every second day from day 2-8.

(A) OCR was measured at day 8 of differentiation under basal conditions and after sequential addition of the following compounds at indicated final concentrations; oligomycin (3 µM); FCCP (1.5 µM); rotenone (1 µM) and antimycin A (1 µM).

(**B**) Outliers were removed based on a Whisker Tukey test of the OCR data for each time point in each well, before calculation of basal respiration, ATP production, maximal respiration and spare respiratory capacity according to the manufacturer's protocol. Results are presented as geometric mean ± 95% confidence interval (n=22-24 replicate wells in a 96-well plate).

(**C**) 3T3-L1 preadipocytes were induced to differentiate and transfected with *Slc7a10* expression plasmid or empty vector on every second day of differentiation (days 2, 4 and 6) and mRNA was collected on day 8. Slc7a10 expression was quantified by qPCR relative to Rsp13 expression (n=3)

**, p<0.01. ***, p<0.001.

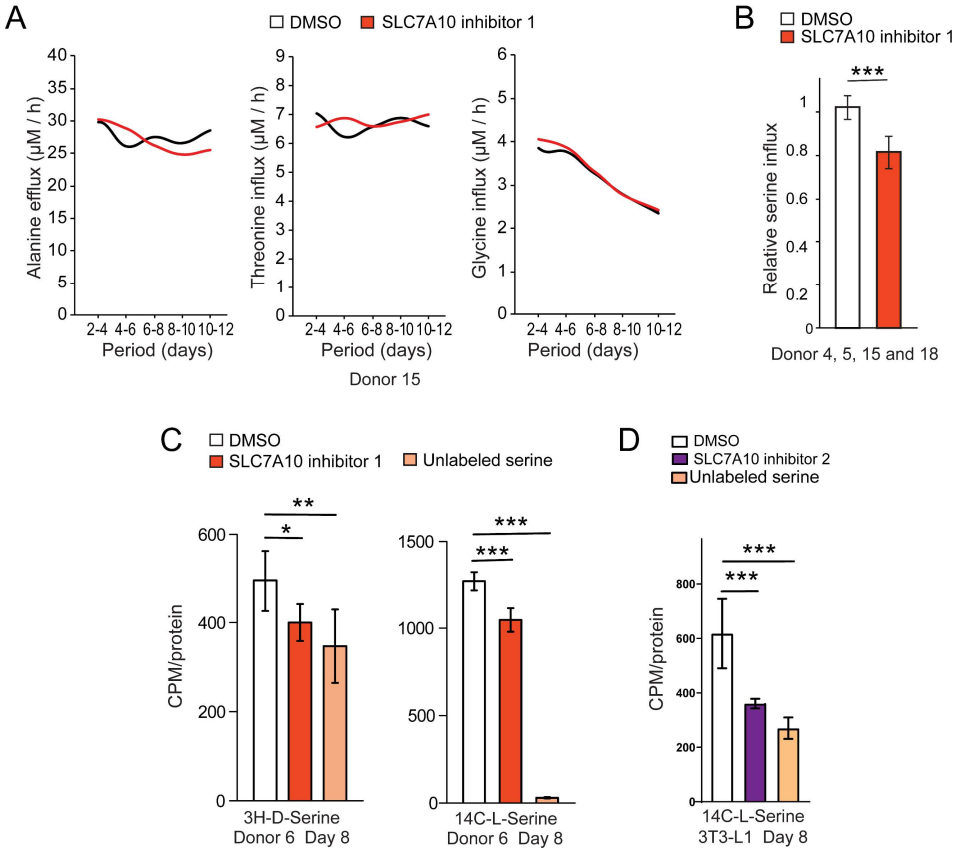

Supplementary Figure 7. Inhibition of SLC7A10 in human primary and mouse adipocytes regulates adipocyte serine uptake and redox status.

(**A**) Changes in alanine, threonine and glycine flux was not alter for hASCs treated with SLC7A10 inhibitor 1 throughout differentiation. Amino acid flux was calculated based on the amino acid concentrations in unconditioned medium and change in concentrations upon cell culture during 48-hour periods. Data for two replicate wells for a representative experiment are shown.

(**B**) The average reduction in serine influx due to SLC7A10 inhibition was calculated (as in A) for fully differentiated hASCs (day 10-12), for replicate experiments in cells from four different people.

(**C**) hASCs were treated with SLC7A10 inhibitor 1 for 30 minutes at day 8 of differentiation. Thereafter, radiolabeled 3H-D-serine (1 µM) or 14C-L-serine (1 µM) was added for 30 minutes and cellular uptake of the radiolabeled amino acids was measured in cell lysate. Unlabeled D-serine and L-serine (100 mM) were used as positive control of uptake inhibition. Data are presented as mean ± SD (n=3-6).

(**D**) 3T3-L1s were treated with SLC7A10 inhibitor 2 for 30 minutes at day 8 of differentiation. Thereafter, radiolabeled 14C-L-serine (1 µM) was added for 30 minutes and cellular uptake of the radiolabeled amino acids was measured in cell lysate. Unlabeled L-serine (100 mM) were used as positive control of uptake inhibition. Data are presented as mean ± SD (n=6).

*, $p<0.05$, **, $p<0.01$. ***, $p<0.001$.

Supplementary References

1. Mi H, Muruganujan A, Huang X, Ebert D, Mills C, Guo X, et al. Protocol Update for large-scale genome and gene function analysis with the PANTHER classification system (v.14.0). Nat Protoc [Internet]. 2019 Mar 25 [cited 2019 Apr 4];14(3):703–21. Available from: http://www.nature.com/articles/s41596-019-0128-8
2. Eden E, Navon R, Steinfeld I, Lipson D, Yakhini Z. GOrilla: a tool for discovery and visualization of enriched GO terms in ranked gene lists. BMC Bioinformatics [Internet]. 2009 Feb 3 [cited 2018 Jan 31];10(1):48. Available from: http://www.ncbi.nlm.nih.gov/pubmed/19192299
3. Supek F, Bošnjak M, Škunca N, Šmuc T. REVIGO Summarizes and Visualizes Long Lists of Gene Ontology Terms. Gibas C, editor. PLoS One [Internet]. 2011 Jul 18 [cited 2019 Mar 27];6(7):e21800. Available from: https://dx.plos.org/10.1371/journal.pone.0021800